SANDIA REPORT

SAND2007-1643
Unlimited Release
Printed March 2007

Fuel Traps:
Mapping Stability via Water Association

Susan L. Rempe, Dubravko Sabo, Jacalyn S. Clawson, Jeffery A. Greathouse, Kevin Leung, Randall T. Cygan, Marcus G. Martin, Todd M. Alam, Sameer Varma

Sandia National Laboratories

Fuel Traps:
Mapping Stability via Water Association

Susan Rempe, Dubravko Sabo, Marcus Martin, Sameer Varma
Computational Bioscience

Jacalyn Clawson, Todd Alam

Electronic and Nanostructured Materials

Jeffery Greathouse, Randall Cygan

Geochemistry

Kevin Leung

Surface and Interface Sciences

Sandia National Laboratories, P.O. Box 5800, Albuquerque, NM 87185-0895

Abstract

Hydrogen storage is a key enabling technology required for attaining a hydrogen-based economy. Fundamental research can reveal the underlying principles controlling hydrogen uptake and release by storage materials, and also aid in characterizing and designing novel storage materials. New ideas for hydrogen storage materials come from exploiting the properties of hydrophobic hydration, which refers to water's ability to stabilize, by its mode of association, specific structures under specific conditions. Although hydrogen was always considered too small to support the formation of solid clathrate hydrate structures, exciting new experiments [Mao, et al. PNAS, 2004] show that water traps hydrogen molecules at conditions of low temperatures and moderate pressures. Hydrogen release is accomplished by simple warming. While these experiments lend credibility to the idea that water could form an environmentally attractive alternative storage compound for hydrogen fuel, which would advance our nation's goals of attaining a hydrogen-based economy, much work is yet required to understand and realize the full potential of clathrate hydrates for hydrogen storage. Here we undertake theoretical studies of hydrogen in water to establish a firm foundation for predictive work on clathrate hydrate H_2 storage capabilities. Using molecular simulation and statistical mechanical theories based in part on quantum mechanical descriptions of molecular interactions, we characterize the interactions between hydrogen and liquid water in terms of structural and thermodynamic properties. In the process we validate classical force field models of hydrogen in water and discover new features of hydrophobic hydration that impact problems in both energy technology and biology. Finally, we predict hydrogen occupancy in the small and large cages of hydrogen clathrate hydrates, a property unresolved by previous experimental and theoretical work.

4

Contents

List of Figures

8

List of Tables

Chapter 1

Introduction

Clathrate hydrates belong to a group of inclusion solid state compounds in which hydrogen-bonded water molecules form host polyhedra cages that trap hydrophobic guest molecules.[1] The thermodynamic stability of the clathrate hydrate lattice depends on both the identity of the guest molecule(s) and the specific conditions of temperature and pressure. While methane clathrate hydrates have long been known to exist in arctic soils and beneath the sea floor, recent experimental results have demonstrated the possibility of synthesizing a whole new class of clathrate hydrates that trap hydrogen gas.[2, 3] Excitement over hydrogen clathrate hydrates centers around their potential use as an environmentally attractive alternative material for hydrogen storage.[4]

Experimental investigations show that hydrogen clathrate hydrates crystallize by forming the so-called sII type cubic structure illustrated in Fig. 1.1. A unit cell of the sII clathrate consists of 16 "small" dodecahedral cages, polyhedrons with 12 pentagonal faces (5^{12}) made up of 20 water molecules, and 8 "large" hexakaidecahedral cages, polyhedrons with 12 pentagonal and 4 hexagonal faces ($5^{12}6^4$) made up of 28 water molecules.[5, 6] In order to be a good candidate for a storage medium, clathrate hydrates must uptake a substantial amount of hydrogen into the cages of the clathrate structure.
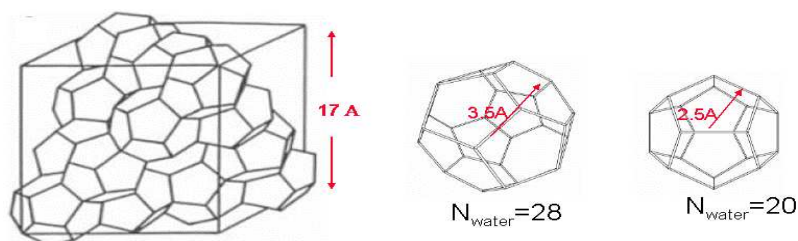
Figure 1.1. The unit cell of the crystalline sII type hydrogen clathrate hydrate lattice and its component "large" and "small" cages formed by hydrogen-bonded water molecules.[3]

Studies to identify the hydrogen occupancy of pure hydrogen clathrate cages have been inconclusive. Initial experiments[3] and theoretical studies based on quantum mechanically derived forces[5, 7] have reported double (quadruple) occupancy of the small (large) cages, while more recent experiments[8] and theoretical studies based on classical force fields[9] have instead found only single hydrogen molecule occupancy in the small cages. Double occupancy by hydrogen molecules in the small cages accompanied by quadruple occupancy in the large cages leads to a 5.3 weight per cent mass storage capacity, which meets the 2006 DOE target for hydrogen fuel storage. Single occupancy in the small cages, however, reduces the mass ratio to 3.9 weight per cent. To evaluate these materials for their potential to store hydrogen, the distribution of hydrogen in the clathrate hydrate cages must be unambiguously determined.

Further difficulties in developing hydrogen clathrate hydrates as hydrogen storage materials arise due to the harsh thermodynamic conditions required for clathrate formation. Initial experiments showed that crystallization of hydrogen clathrate hydrates occurs under harsh conditions of high pressure (2000 atm) and moderately low temperature (249 K).[3] With further reduction in temperature below 140 K, hydrogen clathrate hydrates can be preserved at ambient pressures. Promising data from more recent work demonstrates that additives, such as tetrahydrofuran, stabilize clathrate hydrates under more moderate conditions.[10] Unfortunately, X-ray[10] and neutron[11] diffraction studies show that this particular additive displaces hydrogen molecules, leading to diminished potential storage capacity of the clathrate structure. In order to be of practical utility for hydrogen storage, hydrogen clathrates need to satisfy two criteria: first, they need to be synthesized and preserved under more moderate thermodynamic conditions, ideally under ambient temperature and pressure; second, they should maximize hydrogen occupancy.

Molecular studies can aid the search for additive molecules that simultaneously maximize hydrogen occupancy and stabilize the clathrate structure at moderate thermodynamic conditions. In addition, molecular studies can confirm the mass ratio of hydrogen occupying both pure clathrates and clathrates with additives. A necessary prerequisite for molecular studies, however, is identification of a reliable force field model for describing interactions in the hydrogen water system.

Here we undertake an in-depth theoretical study of the molecular properties of hydrogen in liquid water to identify a force field appropriate for studies of clathrate hydrate systems. Furthermore, we examine the fundamental structural and thermodyamic properties of hydrophobic hydration, in general, since hydrophobic effects are broadly important in both biology and in energy technology. Hydrophobic effects,[12] for example, are one of the dominant driving forces for protein folding[13, 14] and other self-assembly processes such as formation of micelles and lipid bilayers.[15]

In Chapter 2, we report on our studies of the structural properties of a hydrogen molecule dissolved in liquid water. The radial distribution function, coordination number and coordination number distribution are calculated using different representations of the interatomic forces within molecular dynamics, Monte Carlo and *ab initio* molecular dynamics simulation frameworks. Although structural details differ in the radial distribution functions

generated from the different force fields, all approaches agree that the average and most probable number of water molecules occupying the inner hydration sphere around hydrogen is 16. Furthermore, all results exclude the possibility of clathrate-like organization of water molecules around the hydrophobic molecular hydrogen solute despite the common view that hydrophobic solutes support such structures in liquid water.

In Chapter 3, we report on the thermodynamic properties of hydrogen gas in liquid water obtained using Monte Carlo molecular simulation and the quasichemical theory. The free energy of hydrogen hydration in liquid water obtained by Monte Carlo simulations is in excellent agreement with the experimental result, indicating that the classical force field employed in this work provides an adequate description of the intermolecular interactions between water-water and water-hydrogen molecules, at least for the studies of structural and thermodynamic properties. Estimates of the hydrogen hydration free energy within the framework of the quasichemical theory also agree reasonably well with experiment, after corrections are applied for approximations used in a primitive implementation of the theory. Furthermore, these theoretical results reveal that the total free energy results from a balance between chemical association within the inner hydration shell and molecular packing around it, an effect also seen in the hydration of water.[16, 17] This may suggest that the local structure of water around the hydrogen solute is only weakly perturbed from its bulk structure and thermodynamically resembles bulk water.

Finally, in Chapter 4, the H_2 occupancy in the cages of type-II hydrogen clathrate is determined using quantum chemistry calculations. Reaction energies show that the small (D-5^{12}) cage is singly occupied while the large (H-$5^{12}6^4$) favors a four-fold occupancy, in agreement with the results of recent experimental studies.

To summarize, we have carried out theoretical studies of hydrogen interacting with liquid water and pure clathrate hydrate cages to lay the groundwork for future work on clathrate hydrates, in particular, and hydrophobic hydration phenomena important both to energy technology and biology, in general. As a consequence of our work, we have identified a reliable force field that faithfully represents structural and thermodynamic properties due to interactions between hydrogen and water. Furthermore, we have gained new molecular insight into the structural and thermodynamic features of hydrophobic hydration. Finally, we have confirmed the distribution of hydrogen gas molecules in the small and large cages of pure hydrogen clathrate hydrates.

References

[1] E. D. Sloan. *Clathrate Hydrates of Natural Gases*. Marcel Dekker Inc., New York, 2nd edition, 1998.

[2] Y. A. Dyadin, E. D. Larinov, A. Y. Manakov, F. V. Zhurko, E. Y. Aladko, T. V. Mikina, and V. Y. Komarov. *Mendeleev Commun.*, 5:209, 1999.

[3] W. L. Mao, H.-K. Mao, A. F. Goncharov, V. V. Struzhkin, Q. Guo, J. Hu, J. Shu, R. J. Hemley, M. Somayazulu, and Y. Zhao. *Science*, 297:2247, 2002.

[4] W. L. Mao and H.-K. Mao. *Proc. Natl. Acad. Sci. U.S.A.*, 101:708, 2004.

[5] S. Patchkovskii and J. S. Tse. *Proc. Natl. Acad. Sci. U.S.A.*, 100:14645, 2003.

[6] B. C. Chakoumakos, C. J. Rawn, A. J. Rondinone, L. A. Stern, S. Circone, S. H. Kirby, Y. Ishii, C. Y. Jones, and B. H. Toby. *Can. J. Phys.*, 81:183, 2003.

[7] M. H. F. Sluiter, H. Adachi, R. V. Belosludov, V. R. Belosludov, and Y. Kawazoe. *Mater. Trans.*, 45:1452, 2004.

[8] K. A. Lokshin, Y. Zhao, D. He, W. L. Mao, H.-K. Mao, R. J. Hemley, M. V. Lobanov, and M. Greenblatt. *Phys. Rev. Lett.*, 93:125503, 2004.

[9] S. Alavi, J. A. Ripmeester, and D. D. Klug. *J. Chem. Phys.*, 123:024507, 2005.

[10] L. J. Florusse, C. J. Peters, J. Schoonman, K. C. Hester, C. A. Koh, S. F. Dec, K. N. Marsh, and E. D. Sloan. *Science*, 306:469, 2004.

[11] K. C. Hester, T. A. Strobel, E. D. Sloan, C. A. Koh, A. Huq, and A. J. Schultz. *J. Phys. Chem. B*, 110:14024, 2006.

[12] C. Tanford. *Protein Sci.*, 6:1358, 1997.

[13] W. Kauzmann. *Adv. Protein Chem.*, 14:1, 1958.

[14] K. A. Dill. *Biochemistry*, 29:7133, 1990.

[15] C. Tanford. *Science*, 200:1012, 1978.

[16] D. Asthagiri, L. R. Pratt, and J. D. Kress. *Phys. Rev. E*, 68:041505, 2003.

[17] A. Paliwal, D. Asthagiri, L. R. Pratt, H. S. Ashbaugh, and M. E. Paulaitis. *J. Chem. Phys.*, 124:224502, 2006.

Chapter 2

Molecular studies of the structural properties of hydrogen gas in bulk water

2.1 Introduction

Hydrophobic hydration phenomena are the subject of active research because of their importance in biology and energy technology. In biology, hydrophobic effects play a fundamental role in understanding protein structure, stability and function.[1, 2, 3] For example, hydrophobic interactions are considered to be one of the dominant forces driving protein folding as well as formation of micelles and bilayer membranes.[4] In efforts to develop energy technology, hydrophobic interactions are recognized for their role in stabilizing hydrophobic gas particles, such as methane, in solid water structures. Although these solid clathrate hydrates cause difficulties in oil and gas exploration because they tend to clog pipelines,[5] the gases stored within these structures also hold potential as a fuel source.[6]

While different meanings have been applied to describe the notion of the hydrophobic effect in the literature,[2, 7] in the context of the present work we refer to the hydrophobic effect as a phenomenon that involves an arrangement of water molecules around a nonpolar solute. On the macroscopic scale, a hydrophobic solute appears to "dislike" water as is, for example, the case in the separation of oil from water. On the microscopic scale involving dissolution of small hydrophobic particles, the presence of a nonpolar solute is associated with disruption of energetically favorable hydrogen bond networks, leading water molecules to "push away" the solute. A more specific structural explanation of the hydrophobic effect has been invoked to explain the observation that dissolution of two hydrophobic Ar gas atoms yields the same change in entropy as dissolution of hydrophilic KCl salt.[8] The structural explanation is that water forms an ordered arrangement around the hydrophobic solute, leading to formation of a local clathrate-like structure.[9]

True clathrate structures formed from water and hydrophobic gases exist under specific thermodynamic conditions. These clathrate hydrates belong to a group of inclusion

solid state compounds in which the guest (hydrophobic) molecule occupies the host poly-hedra cages that are formed by hydrogen bonded water molecules.[10] A signature of the existence of clathrates comes from the regular numbers of water molecules forming the host cages, the sequence of possibilities (20, 24, 28, etc.) sometimes referred to as "magic" numbers. One can think of clathrate hydrates as solid solutions of water that trap hydrophobic molecules. Without the presence of the guest molecule(s) and the existence of suitable thermal parameters (temperature and pressure) the clathrate hydrate lattice would be thermodynamically unstable, that is, it would not exist.

Recent experimental results have demonstrated the possibility of synthesizing a whole new class of clathrate hydrates, hydrogen clathrate hydrates,[11, 12] and raised the prospect of utilizing them as an alternative storage material for hydrogen fuel.[13] The synthesized hydrogen clathrate was found to crystallize by forming the so-called sII type clathrate cubic structure. A unit cell of the sII clathrate consists of 16 "small" (dodecahedral-5^{12}) cages made up of 20 water molecules (see Fig. 2.9a) and 8 "large" (hexakaidecahedral-$5^{12}6^4$) cages made up of 28 water molecules (see Fig. 2.9b).[14, 15]

The question of what number of hydrogen molecules can be accomodated in the cages of the clathrate is of practical importance because it determines the hydrogen storage ca-pacity of the hydrogen clathrates. Experimental and theoretical studies of the hydrogen occupancy of the hydrogen clathrate cages have been inconclusive on this important issue. Mao $et\ al.$[12] found that the molecular ratio of H_2 to H_2O was $R = 0.45 \pm 0.05$. Such a value suggests that 2 H_2 molecules occupy the small cages and 4 H_2 molecules occupy the large cages and yields a H_2:H_2O mass ratio of 5.2%. These experimental findings were con-firmed by theoretical work of Patchkovskii and Tse.[14] More recently, neutron diffraction studies of the hydrogen clathrate with D_2 guests have reported single and quadruple occu-pancy of the small and large cages by D_2 molecules, respectively.[16] This cage-occupation arrangement corresponds to H_2:H_2O mass ratio of only 3.9%. It was also shown that the oc-cupation number of the large cages decreases with increasing temperature of the clathrate. Experimental results obtained by neutron diffraction studies were in qualitative agreement, regarding the cage occupancy, with recent molecular dynamics simulations.[17]

Another important consideration involves the conditions under which the clathrates are stable. Hydrogen clathrates were synthesized at relatively harsh conditions: high pressures ~ 2000 atm and moderately low temperatures ~ 249 K.[12] It was observed that the hy-drogen clathrate preserved its stability at ambient pressure (1 atm) and temperatures lower than 140 K, but at ambient pressure and temperatures of 140 K and higher, the clathrate released the stored hydrogen. In order to be of practical interest for hydrogen storage, the hydrogen clathrates need to be stabilized under more moderate conditions, ideally un-der standard conditions (1 atm and 298 K). Binary sII clathrate hydrates containing H_2 and THF molecules were synthesized and stabilized at much lower pressure (~ 50 atm at 280 K) than the pure hydrogen clathrate (~ 2000 atm at 280 K).[18] The presence of the additive molecule (THF) enables the stabilization of the clathrate at relatively moderate conditions. X-ray diffraction showed that the THF molecules occupy the large cages while the H_2 molecules occupy the small cages. Such a cage-occupation arrangement of the guest

molecules, however, diminishes the potential storage capacity of the clathrate.

Recently, Lee *et al.*[19] synthesized binary H_2/THF clathrates at modest pressures by tuning the mole percent (concentration) of THF in the water/H_2 solution. The X-ray diffraction studies of the binary H_2/THF clathrate showed that hydrogen guests occupy small and some large cages while THF guests occupy the remaining large cages. Decreasing the concentration of THF in the solution from 5.6% to 0.15% increases the hydrogen storage capacity from 2.1 wt% to 4.0 wt%. In future work, molecular studies can aid the search for additive molecules that simultaneously maximize hydrogen occupancy and stabilize the clathrate structure at moderate conditions. In addition, molecular studies can confirm the mass ratio of hydrogen occupying both pure clathrates and clathrates with additives.

In the present work, we study the structural properties of hydrogen in liquid water that are relevant to the clathrate phase as well as to the phenomenon of hydrophobic hydration and the associated hydrophobic effect. Our purpose is to acquire a better microscopic understanding of the water-hydrophobic solute systems, in general, and water-hydrogen systems, in particular. Our goals are to obtain structural information about the size and distribution of water clusters around the hydrogen molecule and to gain insight into trapping of hydrogen by water. In the process we will address the proposition that local clathrate-like structures stabilize hydrophobic solutes, such as H_2, in liquid water. In addition, we examine the adequacy of and compare different force fields used to model water-water and water-hydrogen interactions to determine which force field could be used as a point of departure for future studies of hydrogen occupancy and hydrogen clathrate hydrate stability.

The remainder of the paper is organized as follows. In Sec. 2.2 we give a brief review of the computational methods and the model potentials employed to calculate the structural properties of water around the hydrogen molecule. In Sec. 2.3 we present the results including the radial distribution functions, hydration numbers and coordination number distributions. Finally, we summarize our findings in Sec. 2.4.

2.2   Computational Method

In the present section, we describe the computational details of our studies involving the hydrogen molecule in bulk water. The system is studied by three different computational methods and modeled by three different force fields. Molecular dynamics (MD) simulations were performed utilizing the flexible simple point charge (SPC) water model[20, 21] combined with the spherical H_2 model, Monte Carlo (MC) simulations were performed utilizing the extended simple point charge (SPC/E) model potential[22] combined with the 3-site charge H_2 model[17] and *ab initio* molecular dynamics (AIMD) simulations were carried out by calculating forces "on the fly."

Table 2.1. Potential parameters for the flexible SPC water−H$_2$ models utilized in the MD simulations. ^{a}The potential parameters between unlike atoms are determined by simple combination rules (see text).

Atom type	Description	q (e)	$\sigma_{ii}{}^a$ (Å)	$\varepsilon_{ii}{}^a$ (kcal·mol^{-1})
H$_2$	Clathrate small cage (5^{12})	0	3.14	0.0190
	Clathrate large cage ($5^{12}6^4$)	0	3.12	0.0188
O^W	Water O	-0.82	3.17	0.155
H^W	Water H	0.41	0	0

2.2.1 Molecular dynamics simulation

A series of MD simulations were performed to investigate the hydration of H$_2$ in bulk water. The flexible SPC water model potential[20, 21] was used for all simulations. Several H$_2$−H$_2$O parameters were used to compare their validity. All H$_2$ models considered in the present work treat the hydrogen molecule as a single sphere with no atomic charge. A difference between the models lies in the Lennard-Jones parameters. Two models were obtained from studies of hydrogen clathrates[23] assuming single H$_2$ occupancy in the cages. All potential parameters are listed in Table 2.1, while the potential energy between two monomers, i and j, is given by

$$V_{ij} = \sum_{m \in i} \sum_{n \in j} \frac{q_m q_n}{r_{mn}} + 4\varepsilon_{ij} \left[\left(\frac{\sigma_{ij}}{r_{ij}} \right)^{12} - \left(\frac{\sigma_{ij}}{r_{ij}} \right)^6 \right], \tag{2.1}$$

where m and n are the charge sites on monomers i and j, respectively, q_m (q_n) is the atomic charge on charge site m associated with monomer i (n associated with monomer j), r_{mn} is the distance between charges on different molecules, r_{ij} is the distance between atomic sites on two monomers and ε_{ij} and σ_{ij} are Lennard-Jones parameters. Simple combination rules (Lorentz-Berthelot)[24, 25] were used to determine the O^W−H$_2$ interaction energy [O^W (H^W) denotes the oxygen (hydrogen) atom in the water molecule]. Intramolecular degrees of freedom (bond stretch and angle bend) of water molecules were also included in the simulations.[20, 21]

   All MD simulations were performed using the LAMMPS code[26] by employing periodic boundary conditions. Short-range interactions were calculated every 0.5 fs while the long-range portion of the electrostatic interactions were calculated every 1.0 fs by implementing a particle-particle particle-mesh technique.[27] Data were collected during a 1.0-ns production NVE (microcanonical ensemble) stage which followed a 0.5-ns equilibration stage. Velocity scaling was used initially with a target temperature of 300 K. Each

water box was constructed to give a water density of 1.0 gcm^{-3}. Data were obtained for boxes containing 64, 114, and 215 waters corresponding to box lengths ranging from 12.4 Å-18.6 Å. A single H_2 particle was then inserted into each box and new simulations were performed.

2.2.2   Classical Monte Carlo simulation

The properties of interest were computed using the MCCCS (Monte Carlo for complex chemical systems) Towhee simulation package.[28] Simulations were carried out in the canonical (NVT) ensemble at a temperature of 300 K and the isothermal-isobaric (NpT) ensemble at a temperature of 300 K and a pressure of 1 atm. The simulation box utilized in the NVT ensemble was a cubic box, with sides of length 17 Å and periodic boundary conditions, which contained 1 H_2 molecule surrounded by 136 water molecules. The same number of molecules was used in the NpT ensemble simulations. Simulations were divided into two phases: an equilibration phase that consisted of 400,000 Monte Carlo cycles (one cycle corresponds to N moves where N is the number of molecules in the system) and an accumulation phase, for which the results are reported, that consisted of 1,000,000 cycles.

The "menu" of the Monte Carlo moves for the NpT ensemble consist of volume changes, configurational-bias single box molecule reinsertion moves (a move that takes a molecule out of a box and tries to place it back into the same box by growing it using coupled-decoupled configurational-bias (CDCB) Monte Carlo),[29, 30] translation of the center of mass, and rotation about the center of mass. The Monte Carlo moves for the NVT ensemble consist of translation of the center of mass and rotation about the center of mass of the molecules.

Interactions between molecules in the system were modeled by the SPC/E potential, the functional form given by Eq. (2.1). The SPC/E potential treats the water molecules as rigid bodies. Unlike the flexible SPC water potential utilized in the MD simulations, which treats the H_2 molecules as spheres without charge, this potential treats the H_2 molecule as a rigid body with a bond length of 0.7414 Å and a quadrupole moment equal to the experimental gas-phase value.[17] The charges are located on the hydrogen nuclei and at the center of mass of the H_2 molecule (see Table 2.2).

2.2.3   *Ab initio* molecular dynamics simulation

For all simulations presented here, we utilized the Vienna *ab initio* simulation package (VASP)[31, 32] based on a generalized gradient approximation (GGA) of Perdew and Wang (PW91)[33, 34] to a plane wave density functional theory with the ultrasoft Vanderbilt pseudopotentials.[35, 36] A kinetic energy cut-off of 36.75 Ry defined the plane wave basis expansions of the valence electronic wave functions.

Table 2.2. Potential parameters for SPC/E water−rigid H_2 molecule model utilized in the MC simulations. These parameters were taken from Ref. [17]. [a]The potential parameters between unlike atoms are determined by simple combination rules (see text).

Atom type	Description	q (e)	$\sigma_{ii}{}^a$ (Å)	$\varepsilon_{ii}{}^a$ (kcal·mol^{-1})
O^W	Water O	-0.8476	3.166	0.1554
H^W	Water H	0.4238	0.000	0.0000
H^A	H in H_2	0.4932	0.000	0.0000
H_2^{CM}	center of mass of H_2	-0.9864	3.038	0.0682

The system simulated by AIMD consisted of 1 H_2 molecule and 32 water molecules in a cubic box with sides of length 9.865 Å in periodic boundary conditions. An initial structure of the system was obtained from a previous study of Kr(aq)[7] where the Kr atom was replaced with a hydrogen molecule. All hydrogen atoms in the system were replaced by deuterium atoms.

The system was equilibrated in the NVT ensemble for the first 11.83 ps at a temperature of 300 K and the equations of motion were integrated in time steps of 1 fs. The production phase was carried out in the NVE ensemble for an additional 18.08 ps where a time step of 0.5 fs was used for integrating the equations of motion.
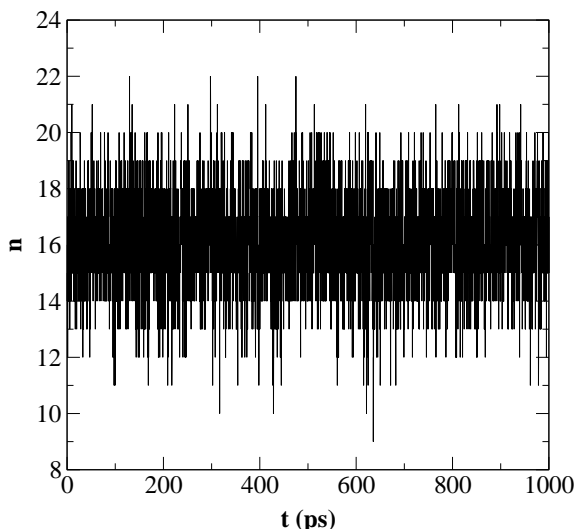
Figure 2.1. Water coordination number (n) of the hydrogen molecule as a function of time obtained by molecular dynamics.

23

2.3   Results and discussion

In this section, we present the results of MD, MC and AIMD simulations carried out on the hydrogen molecule solvated in water. Details about the calculations were given in Section 2.2.

2.3.1   Molecular dynamics

Here we only report the results obtained by simulating the system consisting of 1 hydrogen and 215 water molecules in the simulation box. Similar results were obtained by simulating the system with 64 and 114 water molecules.

Figure 2.1 shows an instantaneous number of water molecules that surround the hydrogen molecule within the sphere of radius $r = 4.96$ Å (first hydration shell). The number of water molecules that cluster around the hydrogen molecule varies from 9 to 22.
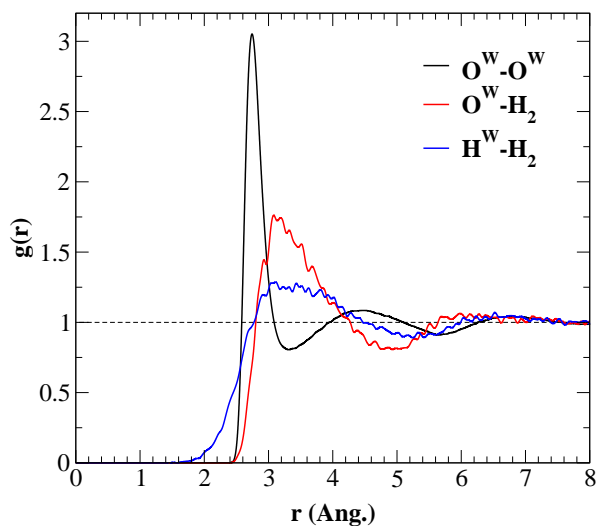
Figure 2.2. Radial distribution functions obtained by the molecular dynamics simulation. Water oxygen (O^W)−water oxygen (O^W) [black line], water oxygen (O^W)−hydrogen molecule (H_2) [red line] and water hydrogen (H^W)−hydrogen molecule (H_2) [blue line] radial distribution functions. Radius r is given in units of Å.

The hydration shell around H_2 was studied by examining radial distribution functions[25] of $O^W - H_2$ and $H^W - H_2$ pairs. The radial distribution functions are shown in Fig. 2.2. Both

O^W-H_2 and H^W-H_2 radial distribution functions display first maxima around 3.2 Å. This is typical structural behavior of water near a small nonpolar (hydrophobic) solute, that is, a well-known feature of hydrophobic hydration (see Ref. [37] and references therein). Although an analysis of the water-water (O^W-O^W) radial distribution function in the system reveals bulk-like structure of water, in the vicinity of a small hydrophobic solute, such as a hydrogen molecule, water molecules are "pushed" further away from the solute, and arrange themselves in such a way that their HOH planes lie almost parallel to the solute surface.[38] In other words, water molecules adopt a preferential orientation near a nonpolar solute and they tend to straddle the solute surface.[39] In this way they preserve the most favorable hydrogen-bonding interaction among themselves in which the number of hydrogen bonds is maximized.

A tail in the H^W-H_2 radial distribution function present at the shorter distances (see Fig. 2.2, 1.6 Å $\leq r \leq$ 2.6 Å) indicates that, on average, water hydrogens lie slightly closer to the solute center than water oxygens. This orientation of the water molecules results in the net positive electrostatic potential found at the center of the solute.[38]
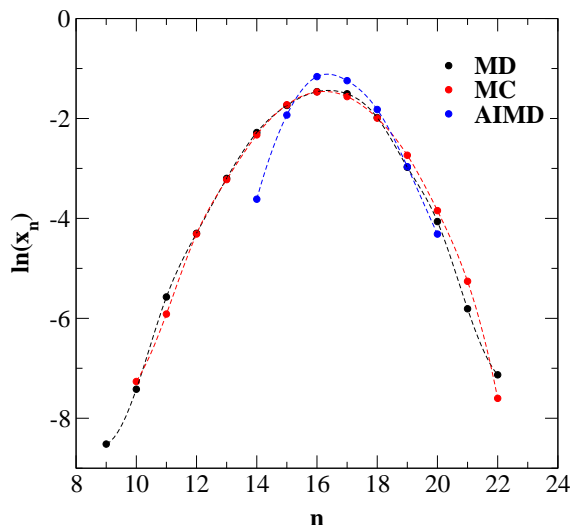
Figure 2.3. Probability distributions of hydration−shell structures with n water molecules surrounding the H_2 molecule yielded from the MD (black symbols), MC (red symbols) and AIMD (blue symbols) simulations. The hydration−shell boundary is defined at $r = 4.96$ Å for MD and MC simulations while for AIMD simulations it is defined at $r = 4.90$Å.

We estimate another property related to structure, the coordination number $\langle n \rangle$. The coordination number, the average number of water molecules that lie within the radius $r = 4.96$ Å around a solute, was obtained by integrating the O^W-H_2 radial distribution function from zero to the first minimum (r$\in$[0, 4.96] Å). Integration yielded a numerical

value $\langle n \rangle = 16.4$.

A final structural determination of hydrogen hydration was made using cluster statistics. The probability x_n of finding n water molecules within the first hydrogen hydration shell (4.96Å) was calculated. Snapshots were examined every 0.2 ps. We found that the most probable size of the water cluster surrounding the hydrogen molecule was $n = 16$. This value is consistent with the coordination number estimated above. Figure 2.3 shows a natural logarithm of the probability that a water cluster of a certain size will enclose the hydrogen molecule. Molecular dynamics results are shown with black symbols and they are in excellent agreement with the Monte Carlo results (red symbols).
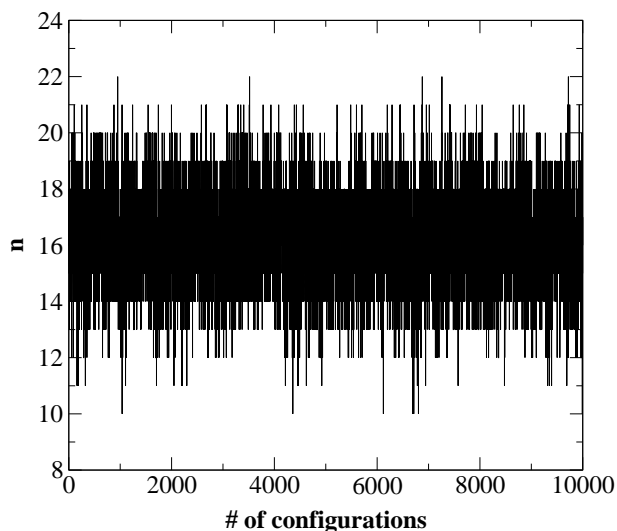
Figure 2.4. Water coordination number (n) of the hydrogen molecule as a function of the Monte Carlo sampled configurations. Each configuration is recorded after 100 Monte Carlo cycles.

2.3.2 Monte Carlo

In the current work, we only present the results obtained by simulations carried out in the NpT ensemble. The NVT ensemble simulations yielded similar results.

The instantaneous coordination number n of the hydrogen molecule in liquid water is shown in Fig. 2.4. During the simulation the system displays "water cages" around the hydrogen molecule ranging in size from 10 to 22, where 10 and 22 water molecule cages are "visited" much less frequently than, for example, the cages made up of 16 or 17 water molecules.

An average coordination number $\langle n \rangle = 16.25 \pm 0.29$ was obtained by integrating the $O^W - H_2^{CM}$ radial distribution function from zero to the first minimum ($r = 4.96$Å; see Fig. 2.5). The uncertainty in $\langle n \rangle$ was obtained as follows. We carried out two simulations in
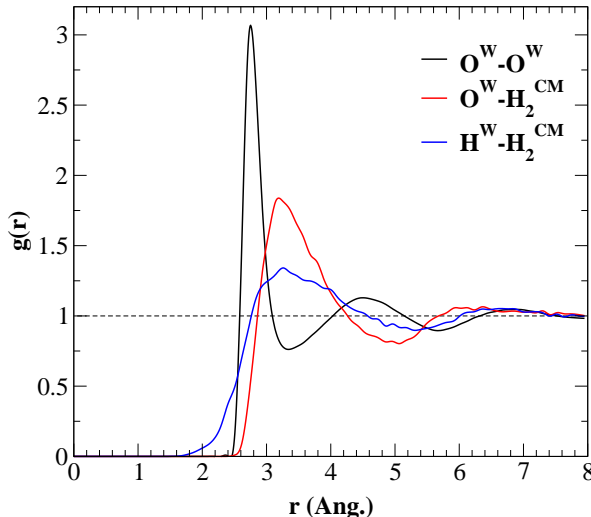
Figure 2.5. Radial distribution functions obtained by the Monte Carlo method. Water oxygen (O^W)−water oxygen (O^W) [black line], water oxygen (O^W)−center of mass of the hydrogen molecule (H_2^{CM}) [red line] and water hydrogen (H^W)−center of mass of the hydrogen molecule (H_2^{CM}) [blue line] radial distribution functions. Radius r is given in units of Å.

the NpT ensemble. For each simulation the radial distribution functions were determined by utilizing a different number of bins[25] (75, 100, and 200). Thus, after averaging over six "measurements" we obtained the above listed value for $\langle n \rangle$. The statistical error of 0.29 corresponds to two standard deviations.

After performing cluster statistics, we found $n = 16$ to be the most probable water structure around H_2. An average most probable coordination number was found as follows. A total number of configurations (10000) was divided in 10 blocks (each block contained 1000 configuration). The most probable coordination number was found for each block and the average most probable coordination number $\langle n_{x_n} \rangle = 16.10 \pm 0.19$ was obtained by averaging over 10 blocks. Statistical error corresponds to two standard deviations. The coordination number distribution x_n is shown in Fig. 2.3. It can be seen that distributions obtained by MC and MD simulations are in excellent agreement for almost the whole range of cluster sizes. The AIMD distribution agrees well with MD and MC distributions near the mode and its right wing. All three methods yield 16 water molecules as the most probable structural arrangement around the H_2 molecule in liquid water. Although we utilize three different force fields in the simulations, the structural properties of water around the

hydrophobic solute turn out to be relatively insensitive to their features.
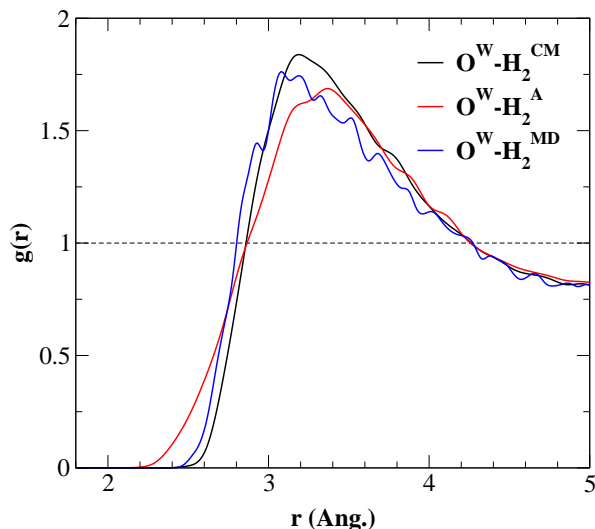
Figure 2.6. Water oxygen (O^W)−center of mass of the hydrogen molecule (H_2^{CM}) [black line], water oxygen (O^W)−hydrogen atom of the hydrogen molecule (H_2^A) [red line] radial distribution functions obtained by the MC simulation. Water oxygen (O^W)−hydrogen molecule (H_2) [blue line] radial distribution function obtained by the MD simulation. The radial distribution functions are only shown up to the first hydration shell. Radius r is given in units of Å.

Complementary structural information about the hydration shell around H_2 was obtained by examining radial distribution functions of $O^W-H_2^{CM}$ and $H^W-H_2^{CM}$ pairs shown in Fig. 2.5. When compared to those obtained by MD simulations (see Fig. 2.2) one can see that they are almost identical. There are small differences between them, however, that can be seen in Fig. 2.6. These differences can be attributed to the nature of the force fields used in the simulations.

A closer look at Fig. 2.6 reveals that $O^W-H_2^{CM}$ (black line; obtained by MC) and $O^W-H_2^{MD}$ (blue line; obtained by MD) radial distribution functions are slightly different for short distances, but they agree for larger distances. The hydrogen molecule is modeled as a rigid body with a finite quadrupole moment (3-site charge H_2 model) in the MC simulations while in the MD simulations as a single sphere without charge (spherical H_2 model). At very large distances ($r \geq 4.0$Å) a water molecule "sees" the hydrogen molecule as a neutral solute (note that the electrostatic potential of a quadrupole moment decreases as $1/r^3$, where r is the distance from the quadrupole moment; see for example Ref. [40]). Thus the reason $O^W-H_2^{CM}$ and $O^W-H_2^{MD}$ radial distribution functions agree at large distances is because hydrogen molecules are seen as neutral species by water molecules in
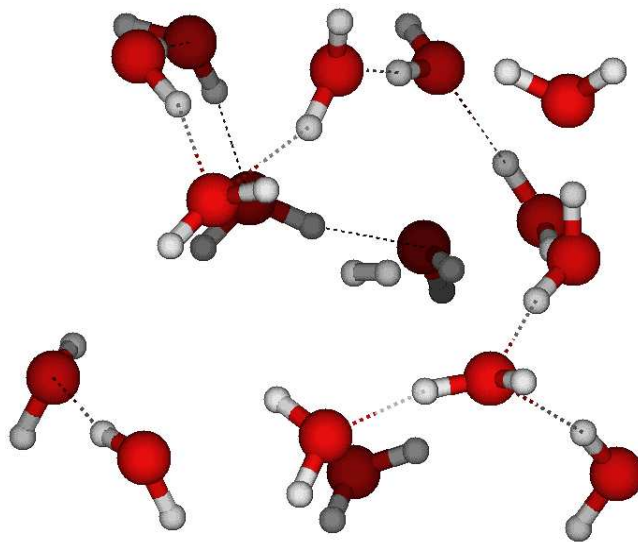
Figure 2.7. Representative snapshot of the 'water cage' structure (made up of 16 water molecules) trapping the hydrogen molecule in liquid water. Hydrogen bonds are depicted by dashed lines. The snapshot was obtained from the Monte Carlo simulation.

both cases.

At medium separations water molecules begin to "sense" the quadrupole moment on the hydrogen molecule. At shorter separations (2.2 Å$\leq r \leq$ 2.8 Å) a water molecule starts to see individual charges on the hydrogen molecule. On average the oxygen atom from the water molecule (O^W), which carries a negative charge, is more likely to come closer to H_2^{MD} as a neutral species than to H_2^{CM} as a negatively charged species. Thus, at short separations the three-site model potential for H_2 is slightly more repulsive than the spherical model potential for H_2 which causes the $O^W - H_2^{MD}$ radial distribution function to be shifted to the left of the $O^W - H_2^{CM}$ radial distribution function. The same phenomenon can be seen when we examine the $O^W - H_2^A$ radial distribution function (red line) in Fig. 2.6 (H_2^A denotes either one of the hydrogen atoms in the hydrogen molecule). A positively charged hydrogen atom on the hydrogen molecule attracts the negatively charged oxygen atom on the water molecule. On average the oxygen atom ($-q$) comes closer to a hydrogen atom ($+q$) than to the center of mass of the hydrogen molecule ($-q$) and the net result is the large tail in $O^W - H_2^A$ radial distribution function at short separations.

We examined a conventional view[41, 42, 2] of hydrophobic hydration that the local structure of liquid water around the hydrophobic solute is clathrate-like. To this end we analyzed snapshots that were sampled during the Monte Carlo simulation. Two representative snapshots displaying a water cluster consisting of 16 and 20 water molecules surrounding the solute are shown in Fig. 2.7 and Fig. 2.8, respectively. These figures suggest that water clusters around a hydrophobic solute are cage-like but not clathrate-like in the sense
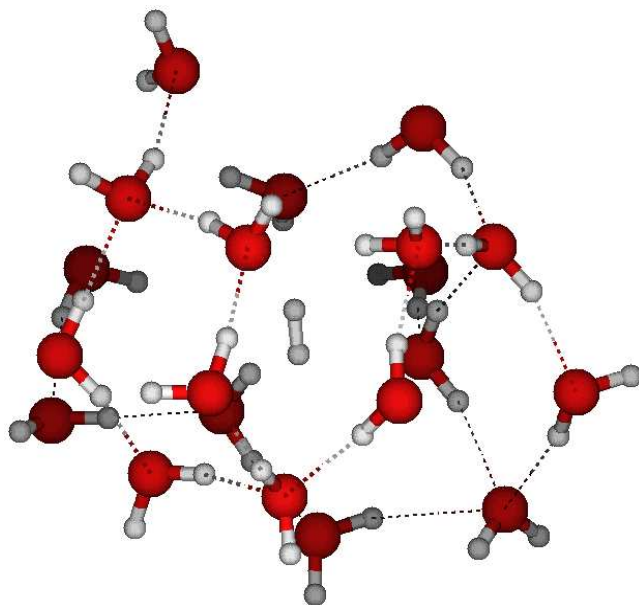
Figure 2.8. Representative snapshot of the 'water cage' structure (made up of 20 water molecules) trapping the hydrogen molecule in liquid water. Hydrogen bonds are depicted by dashed lines. The snapshot was obtained from the Monte Carlo simulation.

that they do not possess the regular-geometric arrangements of the clathrate phase shown in Fig. 2.9. Furthermore, the coordination number distributions shown in Fig. 2.3 indicate that a clathrate-like organization of water clusters around the hydrogen molecule is unlikely to exist. In other words, the magic number water clusters (20, 28–numbers that characterize type II clathrate hydrates) are unlikey to form around the solute in liquid water.

With regard to lack of evidence for clathrate-like structures, our results are consistent with the recent work on the hydration of a krypton atom in liquid water.[7, 43]

2.3.3 *Ab initio* molecular dynamics

The structural analysis presented here was obtained from an 18.08 ps trajectory generated in the microcanonical ensemble after an equilibration period of 11.83 ps at 300 K carried out in the canonical ensemble.

Figure 2.10 (upper trace) shows the instantaneous number of water molecules that surround the hydrogen molecule within the sphere of radius $r = 4.9$ Å (first solvation shell). It can be seen that the size of "water clusters" around the solute fluctuates between 14 and 20 water molecules. The lower trace of Fig. 2.10 shows the instantaneous temperature of the system. Initally the temperature increased and then settled at 310 ± 7 K. The resulting
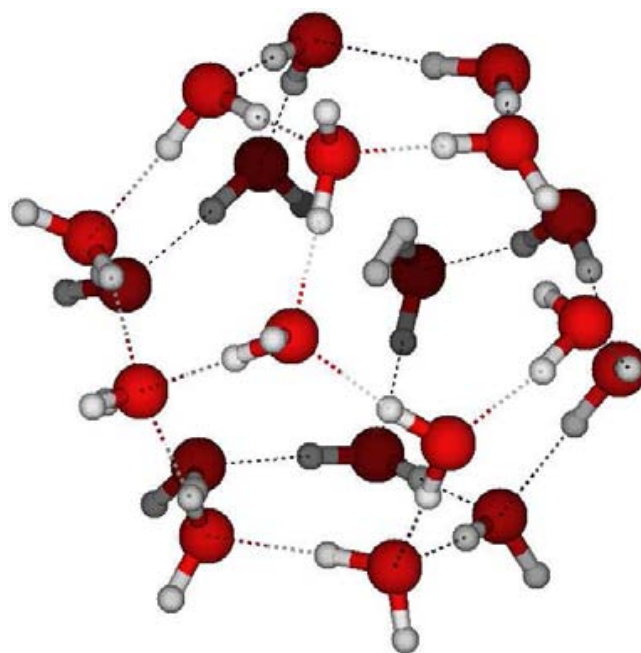
(a)
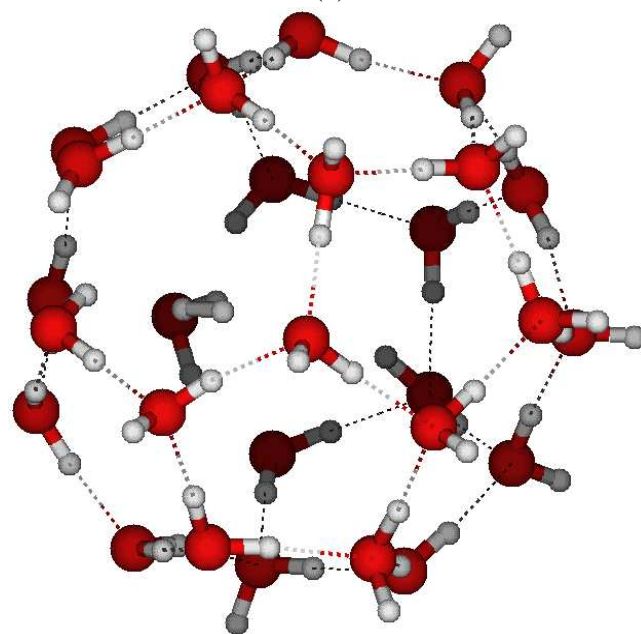
(b)

Figure 2.9. (a) Structure of the small (5^{12}) cage of the type II clathrate hydrate enclosing one hydrogen molecule. The cage consists of 20 water molecules. The notation 5^{12} indicates the number of pentagonal faces (12) making up the polyhedron. (b) Structure of the large ($5^{12}6^4$) cage of the type II clathrate hydrate enclosing one hydrogen molecule. The cage consists of 28 water molecules. The notation $5^{12}6^4$ indicates the number of pentagonal (12) and hexagonal (4) faces making up the polyhedron. Hydrogen bonds are depicted by dashed lines.
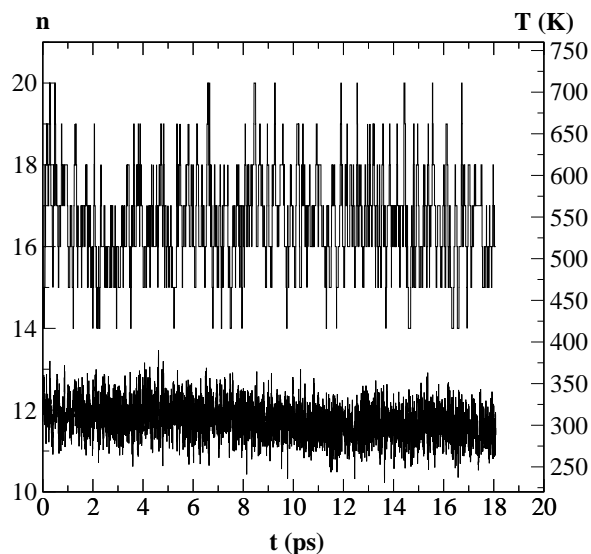
Figure 2.10. Water coordination number (n) of the hydrogen molecule as a function of time (upper trace and left axis) obtained by *ab initio* molecular dynamics. The lower trace shows the temperature of the system as a function of time.

radial distribution functions are shown in Fig. 2.11. When compared to their MD and MC counterparts it can be seen they exhibit the same general characteristics of hydrophobic hydration around small nonpolar solutes, such as bulk-like water structure, water "pushed" away from the solute, and roughly parallel arrangements of water around the hydrophobic solute. More specifically, the classical and AIMD results differ very little at short distances. Small differences appear at larger distances where the AIMD radial distribution functions are more structured than their MD and MC counterparts. The AIMD distribution functions have a higher peak at the first maximum and a "deeper" first minimum. It has also been observed experimentally that the radial distribution functions for the heavier isotope (D_2) are more structured than for the lighter isotope (H_2).[44] While the minima and the maxima are located approximately at the same distances as those in MD and MC radial distribution functions, the maximum of the $O^W - H_2^{CM}$ radial distribution function is slightly shifted toward larger distances (≈ 3.4Å) with respect to the MD and MC counterparts, causing a small separation in the positions of water oxygen and hydrogen atoms and thus tilting of the water molecules away from a planar configuration. Possible reasons for these differences can be identified as:

1. The existence of different charge distributions on the hydrogen molecule and water molecules that lead to more realistic forces in the *ab initio* simulation than those utilized in the classical studies.

2. AIMD simulations that have not been run long enough, which is reflected at least in

32
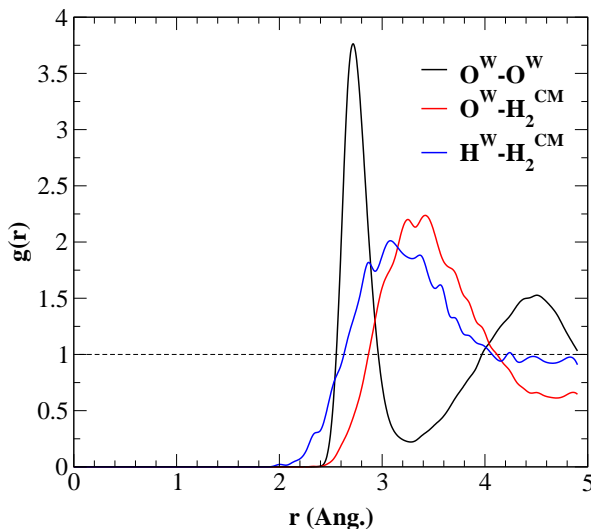
Figure 2.11. Radial distribution functions obtained by *ab initio* molecular dynamics. Water oxygen (O^W)−water oxygen (O^W) [black line], water oxygen (O^W)−center of mass of the hydrogen molecule (H_2^{CM}) [red line] and water hydrogen (H^W)−center of mass of the hydrogen molecule (H_2^{CM}) [blue line] radial distribution functions. Radius r is given in units of Å.

the narrower distribution of structures and larger errors in the wings of the cluster distribution.

Integration of the $O^W - H_2^{CM}$ radial distribution function yields $\langle n \rangle = 16.33$, the same average occupancy of the hydration shell defined by the radius $r = 4.9$Å as found in the classical studies. Similarly, we find that the most probable water cluster structure around the hydrogen molecule is 16. The average most probable coordination number was obtained by dividing the total number of snapshots (taken every 0.5 ps) into blocks of 1000. For each block the most probable coordination number was found and by averaging over all blocks we obtained the average most probable coordination number $\langle n_{x_n} \rangle = 16.46 \pm 0.24$. The error bar corresponds to two standard deviations. The coordination number distribution is shown in Fig. 2.3 by blue symbols.

2.4   Conclusions

We investigated the structural properties of the hydrogen hydration in liquid water by using molecular dynamics, Monte Carlo and *ab initio* molecular dynamics simulation methods with three different force fields: the flexible SPC water model with the spherical H_2 model,

the SPC/E water model with the 3-site charge H_2 model and *ab initio* derived forces, respectively.

We find that the most probable water cluster formed around the hydrogen molecule within the first hydration shell contains 16 water molecules. This result is obtained by all three force fields and confirmed by using clustering statistics and by calculating the coordination number distributions (see Fig. 2.3).

The radial distribution functions obtained by the spherical H_2 and 3-site charge H_2 model exhibit the first maximum at approximately the same distance (≈ 3.2 Å) for both oxygen and hydrogen densities. This is a well-known feature of water structure in the vicinity of the hydrophobic solute and implies that the HOH plane of water molecules is oriented almost tangentially to the solute surface . In other words, the H and O atoms are on average located at the same distance from the solute. At shorter separations (2.2 Å$\leq r \leq$ 2.8 Å) the structural arrangement of water molecules around the hydrogen starts to differ between the two models due to the charge/lack-of-charge distribution on the hydrogen molecule. The oxygen (hydrogen) density obtained by the *ab initio* molecular dynamics is shifted to even longer (shorter) separations with respect to those obtained by the spherical H_2 and 3-site charge H_2 model. These differences may suggest that the classical H_2 models are missing some key components. Accuracy of the two classical force fields models and *ab initio* forces cannot be verified at this point because, to our knowledge, no experimental structural data on aqueous hydrogen is available in the literature.

We note in passing that a conventional view[41, 42, 2] of hydrophobic hydration, which suggests a local clathrate-like organization of water clusters around the hydrophobic solute, does not hold.[7, 43] The coordination number of H_2 in liquid water is 16, a value that differs significantly from the known coordination numbers of true clathrate phases (sI$-20, 24$ or sII$-20, 28$). The clathrate-like picture of hydrophobic hydration in the first hydration shell could be clarified further by an in-depth look at the hydrogen bonding within the first hydration shell and the first and second shells. Additional energetic[45] and geometric (angle)[46] considerations of hydrogen bonding would also help to distinguish first-shell water molecules from those in the bulk. Since the hydration free energy of hydrogen in liquid water is a well-known thermodynamic quantity,[47] calculation of this physical quantity would aid in validating our structural predictions and thus provide additional insight into the hydration of hydrogen in both liquid and clathrate phases. These will be the subjects of future work.

Acknowledgment

References

[1] W. Kauzmann. *Adv. Protein Chem.*, 14:1, 1958.

[2] K. A. Dill. *Biochemistry*, 29:7133, 1990.

[3] C. Tanford. *Protein Sci.*, 6:1358, 1997.

[4] C. Tanford. *Science*, 200:1012, 1978.

[5] I. Chatti, A. Delahaye, L. Fournaison, and J.-P. Petitet. *Energy Convers. Manage.*, 46:1333, 2005.

[6] E. Suess, G. Bohrmann, J. Greinert, and E. Lausch. *Sci. Am.*, 281:76, 1999.

[7] H. S. Ashbaugh, D. Asthagiri, L. R. Pratt, and S. B. Rempe. *Biophys. Chem.*, 105:323, 2003.

[8] H. L. Friedman and C. V. Krishnan. In F. Franks, editor, *Water: A comprehensive treaties*, volume 3, page 1. Plenum Press, New York, 1973.

[9] H. S. Frank and M. W. Evans. *J. Chem. Phys.*, 13:507, 1945.

[10] E. D. Sloan. *Clathrate Hydrates of Natural Gases*. Marcel Dekker Inc., New York, 2nd edition, 1998.

[11] Y. A. Dyadin, E. D. Larinov, A. Y. Manakov, F. V. Zhurko, E. Y. Aladko, T. V. Mikina, and V. Y. Komarov. *Mendeleev Commun.*, 5:209, 1999.

[12] W. L. Mao, H.-K. Mao, A. F. Goncharov, V. V. Struzhkin, Q. Guo, J. Hu, J. Shu, R. J. Hemley, M. Somayazulu, and Y. Zhao. *Science*, 297:2247, 2002.

[13] W. L. Mao and H.-K. Mao. *Proc. Natl. Acad. Sci. U.S.A.*, 101:708, 2004.

[14] S. Patchkovskii and J. S. Tse. *Proc. Natl. Acad. Sci. U.S.A.*, 100:14645, 2003.

[15] B. C. Chakoumakos, C. J. Rawn, A. J. Rondinone, L. A. Stern, S. Circone, S. H. Kirby, Y. Ishii, C. Y. Jones, and B. H. Toby. *Can. J. Phys.*, 81:183, 2003.

[16] K. A. Lokshin, Y. Zhao, D. He, W. L. Mao, H.-K. Mao, R. J. Hemley, M. V. Lobanov, and M. Greenblatt. *Phys. Rev. Lett.*, 93:125503, 2004.

[17] S. Alavi, J. A. Ripmeester, and D. D. Klug. *J. Chem. Phys.*, 123:024507, 2005.

[18] L. J. Florusse, C. J. Peters, J. Schoonman, K. C. Hester, C. A. Koh, S. F. Dec, K. N. Marsh, and E. D. Sloan. *Science*, 306:469, 2004.

[19] H. Lee, J.-W. Lee, D. Y. Kim, J. Park, Y.-T. Seo, H. Zeng, I. L. Moudrakovski, C. I Ratcliffe, and J. A. Ripmeester. *Nature*, 434:743, 2005.

[20] O. Teleman, B. Jönsson, and S. Engström. *Mol. Phys.*, 60:193, 1987.

[21] T. I. Mizan, P. E. Savage, and R. M. Ziff. *J. Phys. Chem.*, 98:13067, 1994.

[22] H. J. C. Berendsen, J. R. Grigera, and T. P. Straatsma. *J. Phys. Chem.*, 91:6269, 1987.

[23] J. B. Klauda and S. I. Sandler. *Chem. Eng. Sci.*, 58:27, 2003.

[24] J. O. Hirschfelder, C. F. Curtiss, and R. B. Bird. *Molecular Theory of Gases and Liquids*. Wiley, New York, 1954. p.168.

[25] M. P. Allen and D. J. Tildesley. *Computer Simulation of Liquids*. Oxford University Press, Oxford, 1996.

[26] S. J. Plimpton. *J. Comp. Phys.*, 117:1, 1995.

[27] S. J. Plimpton, R. D. Pollock, and M. J. Stevens. *Particle-mesh Ewald and rRESPA for parallel molecular dynamics simulations*, 1997. 8th SIAM conference on parallel processing for scientific computing, Minneapolis, MN, USA.

[28] see http://towhee.sourceforge.net.

[29] M. G. Martin and J. I. Siepmann. *J. Phys. Chem. B*, 103:4508, 1999.

[30] D. Frenkel and B. Smit. *Understanding Molecular Simulation*. Academic Press, San Diego, 2002.

[31] G. Kresse and J. Hafner. *Phys. Rev. B*, 47:RC558, 1993.

[32] G. Kresse and J. Furthmüller. *Phys. Rev. B*, 54:11169, 1996.

[33] Y. Wang and J. P. Perdew. *Phys. Rev. B*, 44:13298, 1991.

[34] J. P. Perdew, J. A. Chevary, S. H. Vosko, K. A. Jackson, M. R. Pederson, D. J. Singh, and C. Fiolhais. *Phys. Rev. B*, 46:6671, 1992.

[35] D. Vanderbilt. *Phys. Rev. B*, 41:7892, 1990.

[36] G. Kresse and J. Hafner. *J. Phys. Condens. Matter*, 6:8245, 1994.

[37] L. R. Pratt. *Annu. Rev. Phys. Chem.*, 53:409, 2002.

[38] S. Rajamani, T. Ghosh, and S. Garde. *J. Chem. Phys.*, 120:4457, 2004.

[39] F. H. Stillinger. *Science*, 209:451, 1980.

[40] J. D. Jackson. *Classical Electrodynamics*. John Wiley & Sons, New York, 1975.

[41] Y. Cheng and P. J. Rossky. *Nature*, 392:696, 1998.

[42] D. N. Glew. *J. Phys. Chem.*, 66:605, 1962.

[43] R. A. LaViolette, K. L. Copeland, and L. R. Pratt. *J. Phys. Chem. A*, 107:11267, 2003.

[44] J. Urquidi. Private communication.

[45] A. G. Kalinichev, Y. E. Gorbaty, and A. V. Okhulkov. *J. Mol. Liq.*, 82:57, 1999.

[46] T. M. Raschke and M. Levitt. *Proc. Natl. Acad. Sci. U.S.A.*, 102:6777, 2005.

[47] C. L. Young, editor. *Hydrogen and deuterium (Solubility data series)*, volume 5/6. Pergamon Press, Oxford, 1981.

Chapter 3

Studies of the thermodynamic properties of hydrogen gas in bulk water

3.1 Introduction

Hydrophobic hydration phenomena play a fundamental role in both biology and energy technology. Hydrophobic effects,[1] for example, are one of the dominant driving forces for protein folding[2, 3] and other self-assembly processes such as formation of micelles and lipid bilayers.[4] They are equally important in energy technology for their role in stabilizing hydrophobic gases in clathrate hydrates. Although the best-known methane clathrate hydrates pose a serious risk to oil and gas exploration because they can cause explosions and fires and tend to form costly and hazardous blockages in pipelines,[5] the gases stored within these structures also hold potential as a fuel source.[6] Furthermore, newly discovered hydrogen clathrate hydrates show promise as an alternative storage material for hydrogen fuel.[7]

Clathrate hydrates belong to a group of inclusion solid state compounds in which host polyhedra cages formed by hydrogen bonded water molecules trap hydrophobic guest molecules.[8] Without the guest molecule(s) and suitable thermal parameters (temperature and pressure), the clathrate hydrate lattice would be thermodynamically unstable and not exist. Recent experimental results demonstrate the possibility of synthesizing a whole new class of clathrate hydrates that trap hydrogen, [9, 10] and raise the prospect of utilizing clathrate hydrates for hydrogen fuel storage.[7] Initial results showed that crystallization of hydrogen clathrate hydrates occurs under harsh conditions of high pressure (~ 2000 atm) and moderately low temperature (~ 249 K).[10] With further reduction in temperature below 140 K, hydrogen clathrate hydrates can be preserved at ambient pressures. In order to be of practical utility for hydrogen storage, however, hydrogen clathrates need to satisfy two criteria: first, they need to be synthesized and preserved under more moderate thermodynamic conditions, ideally under ambient temperature and pressure; second, they should maximize hydrogen occupancy.

Efforts aimed at developing hydrogen clathrate hydrates for storage applications face many obstacles. For example, recent work demonstrates that additives, such as tetrahydrofuran, can stabilize clathrate hydrates under more moderate conditions. [11] Unfortunately, X-ray[11] and neutron[12] diffraction studies show that this particular additive displaces hydrogen molecules, leading to diminished potential storage capacity of the clathrate structure. Furthermore, studies to identify hydrogen occupancy of the hydrogen clathrate cages have been inconclusive. While initial experimental[10] and theoretical[13] studies have reported double and quadruple occupancy of the small and large cages, respectively, more recent experimental[12, 14] and theoretical[15, 16] studies have found only single hydrogen molecule occupancy in the small cages.

Molecular studies can aid the search for additive molecules that simultaneously maximize hydrogen occupancy and stabilize the clathrate structure at moderate thermodynamic conditions. In addition, molecular studies can confirm the mass ratio of hydrogen occupying both pure clathrates and clathrates with additives. A necessary prerequisite for molecular studies, however, is identification of a reliable force field model for describing interactions in the hydrogen water system.

Here, we extend our previous molecular investigations[17] of hydrogen in liquid water from the structural into the thermodynamic domain for the purpose of acquiring a better microscopic understanding of water-hydrophobic solute systems, in general, and water-hydrogen systems, in particular. The thermodynamic properties we study are relevant to the clathrate phase as well as to the phenomenon of hydrophobic hydration and the associated hydrophobic interaction. Specific goals are to obtain the net free energy of hydrogen hydration and identify its individual component contributions, and to gain insight into the trapping of hydrogen in water by establishing a direct link between structural and thermal properties. In addition, we evaluate the adequacy of the force field used to model water-water and water-hydrogen interactions to facilitate future molecular studies.

The remainder of the paper is organized as follows. In Sec. 3.2 we give a review of the computational methods and the model potential employed to calculate the thermodynamic properties of hydrogen dissolved in liquid water. In Sec. 3.3 we present the results of our simulations including the complementary results obtained by the quasichemical theory. Finally, we summarize our findings in Sec. 3.4.

3.2 Computational Methods

In the current section, we present the Monte Carlo method along with the force field utilized to calculate the hydration free energy of hydrogen. In addition, we describe how we estimate the net hydration free energy of hydrogen and calculate its individual component contributions within the framework of the quasichemical theory. In the process, we address the strengths and limitations of a primitive evaluation of the thermal properties of a hydrophobic solute and present a scheme for correcting the consequent approximations.

3.2.1 Monte Carlo simulation

The hydration free energy of hydrogen is computed using the MCCCS (Monte Carlo for complex chemical systems) Towhee simulation package (version-4.11.7).[18] Simulations are carried out in the NVT-Gibbs ensemble[19, 20] at a temperature of 298.15 K and the NpT-Gibbs ensemble[21, 20] at a temperature of 298.15 K and a pressure of 1 atm. Two cubic simulation boxes are utilized in both ensembles with an initial box length size of 17 Å and periodic boundary conditions. One box contains 136 water molecules while a second one contains 48 hydrogen molecules. Simulations are divided into two phases: an equilibration phase that consists of 600,000 Monte Carlo cycles (one cycle corresponds to N moves where N is the number of molecules in the system) and an accumulation phase, for which the results are reported, that consists of 300,000 cycles. In both ensembles, we carry out 14 simulations after the equilibration phase such that the final configuration from the previous run is used as the initial configuration in the subsequent run. The value of the free energy is obtained by averaging over 14 resulting "measurements." The free energy is calculated using the following equation,

$$\Delta G = -RT \ ln\frac{\rho_{vap}}{\rho_{liq}}, \tag{3.1}$$

where ρ_{vap} (ρ_{liq}) is the density of hydrogen gas in vapor (liquid), R is the gas constant, and T is the temperature.

The Monte Carlo moves utilized in the NpT-Gibbs ensemble consist of volume changes, configurational-bias single box molecule reinsertion moves (a move that takes a molecule out of a box and tries to place it back into the same box by growing it using coupled-decoupled configurational-bias (CDCB) Monte Carlo),[22, 20] particle exchange moves between two boxes, translation of the center of mass, and rotation about the center of mass of the molecule. The Monte Carlo moves for the NVT-Gibbs ensemble consist of volume changes (the total volume of the system is constant, but the volumes of the subsystems change), translation of the center of mass and rotation about the center of mass of the molecule.

Interactions between molecules in the system are modeled by the SPC/E water-water potential[23] and a 3-site charge H_2 model,[15] with the potential energy form between two monomers, i and j, given by

$$V_{ij} = \sum_{m \in i}\sum_{n \in j} \frac{q_m q_n}{r_{mn}} + 4\varepsilon_{ij}\left[\left(\frac{\sigma_{ij}}{r_{ij}}\right)^{12} - \left(\frac{\sigma_{ij}}{r_{ij}}\right)^{6}\right], \tag{3.2}$$

where m and n are the charge sites on monomers i and j, respectively, q_m (q_n) is the atomic charge on charge site m associated with monomer i (n associated with monomer j), r_{mn} is the distance between charges on different molecules, r_{ij} is the distance between atomic sites on two monomers and ε_{ij} and σ_{ij} are Lennard-Jones parameters. Simple combination rules

40

Table 3.1. Potential parameters for SPC/E water[23]−rigid H_2 molecule model[15] utilized in the MC simulations. The parameters were taken from Ref. [15]. [a]The potential parameters between unlike atoms are determined by simple combination rules (see text).

Atom type	Description	q (e)	$\sigma_{ii}{}^a$ (Å)	$\varepsilon_{ii}{}^a$ (kcal·mol^{-1})
O^W	Water O	-0.8476	3.166	0.1554
H^W	Water H	0.4238	0.000	0.0000
H^A	H in H_2	0.4932	0.000	0.0000
H_2^{CM}	center of mass of H_2	-0.9864	3.038	0.0682

(Lorentz-Berthelot)[24, 25] are used to determine the O^W-H_2 interaction energy, where O^W (H^W) denotes the oxygen (hydrogen) atom in the water molecule. All potential parameters are listed in Table 3.1. Water and hydrogen molecules are treated as rigid bodies. The H_2 molecule is a linear molecule with a bond length of 0.7414 Å and a quadrupole moment equal to the experimental gas-phase value.[15] The charges are located on the hydrogen nuclei and at the center of mass of the H_2 molecule (see Table 3.1).

3.2.2 Quasichemical theory: "A direct approach"[26]

Although the quasichemical theory is described in detail elsewhere, [27, 28, 29] here we review its salient features for completeness. Within the framework of quasichemical theory, the volume associated with a solute-solvent system of interest is partitioned into inner- and outer-shell domains. In the inner shell domain, which can be defined as the region occupied by the innnermost solvent molecules, a solute and n solvent molecules are treated more accurately using quantum chemistry methods. The remaining bulk solvent, defining the outer shell domain, can be treated at a more approximate level by a continuum dielectric model or a classical force field model. This divide-and-conquer approach has proven to be useful in studies of the hydration of ions in water[30, 31, 32, 33, 34, 35, 36] as well as in studies of the selectivity of biological ion channels.[37]

A quasichemical analysis of the system of interest is typically accompanied by structural studies carried out by *ab initio* molecular dynamics or classical force field simulations. These molecular simulations aid in defining a suitable boundary between inner and outer domains of the solute-solvent system to be addressed in the quasichemical analysis. The boundary defines an inner domain where clustering equilibria occur, and the clusters are investigated for their energetic and structural properties. Thus, the quasichemical theory allows one to establish a connection between the thermal and local structural properties of a solute-solvent system.

In the inner shell domain, many solute-solvent interactions, such as those in aqueous electrolyte, can be characterized as chemical associations that are typically far stronger than the thermal energy, kT. In such cases, approximations regarding the nature of the atomic motions in the inner domain and the coupling between inner and outer domains can simplify the thermodynamic analysis and lead to a so-called primitive implementation of the theory. These approximations may not always be reasonable, especially for the solvation of a hydrophobic species such as hydrogen in bulk water. Then such an evaluation of solute thermodynamic properties within the quasichemical framework may give rise to substantial errors, which ultimately can be estimated and corrected. We postpone further discussion of strategies for making such corrections for the end of this section.

The quasichemical formulation enables calculation of the net free energy of hydration in terms of individual contributions arising from local and distant solvation effects. The partial molar Gibbs free energy or chemical potential of the solute (hydrogen) in liquid water can be written as,[38]

$$\mu_{H_2} = RT \ ln \ \left[\frac{\rho_{H_2} \Lambda_{H_2}^3}{q_{H_2}^{int}} \right] + \mu_{H_2}^{ex}, \tag{3.3}$$

where ρ_{H_2} is the number density of the solute, Λ_{H_2} is the thermal de Broglie wavelength and $q_{H_2}^{int}$ is the partition function (without translational degrees of freedom) for a single solute molecule. The first term in Eq. (4.1) is the ideal gas contribution to the chemical potential. In the present work, the quantity of primary interest is the second term, the excess chemical potential, which accounts for intermolecular interactions between the solute and solvent molecules. The excess chemical potential is formally given by the potential distribution theorem[39]

$$\mu_{H_2}^{ex} = -RT \ ln \ \langle\langle e^{-\beta \Delta U_{H_2}} \rangle\rangle_0, \tag{3.4}$$

where ΔU_{H_2} is the potential energy of the interactions between the solvent and solute where the solute is treated as a test particle according to the Widom particle insertion method.[20] The subscript zero associated with $\langle\langle \ldots \rangle\rangle_0$ refers to a test particle ensemble average. Equation (4.2) can be recast in the form useful for the quasichemical approach

$$\beta \mu_{H_2}^{ex} = ln \ x_0 - ln \left\langle\left\langle e^{-\beta \Delta U_{H_2}} \prod_j (1 - b_j) \right\rangle\right\rangle_0, \tag{3.5}$$

where $\beta^{-1} = RT$. The first term on the right hand side of Eq. (3.5) is the inner shell contribution while the second term is the outer shell contribution to the excess chemical potential. x_0 is the probability that the inner shell contains the solute molecule without any solvent molecules and b_j is an indicator function which is one (1) when a solvent molecule j is inside the inner shell and zero (0) otherwise.

3.2.2.1 Inner shell contribution

The inner shell chemical associations (reactions) relevant to the hydration of hydrogen are

$$H_2 + nH_2O \rightleftharpoons H_2(H_2O)_n. \tag{3.6}$$

The probability x_0 can be expressed in terms of equilibrium constants K_n,[28] associated with reactions in Eq. (3.6), as follows

$$x_0 = \frac{1}{1 + \sum_{n \geq 1} K_n \rho_{H_2O}^n}. \tag{3.7}$$

In other words, the coefficients K_n are the usual "products over reactants" chemical equilibrium ratios, and $\rho_{H_2O}^n$ is the solvent number density. The merit of Eq. (3.7) lies in the fact that it is a natural starting point for invoking the following approximation, $K_n \approx K_n^{(0)}$, where $K_n^{(0)}$ are equilibrium ratios for the chemical reactions (3.6) taking place in an ideal gas phase, that is, without consideration of a solution medium. The coefficients $K_n^{(0)}$ can readily be estimated by standard electronic structure computational packages.

Here we calculate the free energy changes for the inner shell reactions utilizing the Gaussian package.[40] Minimum energy structures of the $H_2(H_2O)_n$ clusters as well as of the H_2 and H_2O molecules are determined in the gas phase using the B3LYP hybrid density functional in conjunction with the $6-311+G(2d,p)$ basis set. Resulting structural geometries are confirmed to be stable minima via a standard Hessian analysis, that is, the vibrational frequencies of the clusters and molecules are calculated within a harmonic approximation and checked for the absence of frequencies with imaginary components. Frequencies and zero-point energies are determined at the same level of theory ($6-311+G(2d,p)$ basis set). Single point energies are calculated by using the aug-cc-pvTZ basis. The resulting free energy changes $\Delta G^{(0)} = G_{H_2(H_2O)_n}^{(0)} - (G_{H_2}^{(0)} + nG_{H_2O}^{(0)})$ are shown in Fig. 3.1 for the size of clusters in the range from $n = 12$ to $n = 18$. The density factor ρ_{H_2O} in Eq. (3.7) refers to the actual density of liquid water (at standard conditions) and is accounted for by adding the contribution of $-nRT\ ln\ 1354$ to $\Delta G^{(0)}$.[41]

3.2.2.2 Outer shell contribution

The outer shell contribution to the hydrogen hydration free energy is obtained by treating the solvent external to the clusters in the inner shell as a dielectric continuum. The boundary between the inner and outer shells is determined from the radial distribution function (rdf) calculated in our earlier structural study of the hydrogen molecule in liquid water.[17] The spherical volume defined by a radius of 5.44 Å from the center of mass of the hydrogen

molecule, which corresponds to the average distance between the first minimum (at radius 4.96 Å) and the second maximum of the rdf, contains the inner shell domain. Partial atomic charges required for the numerical solution of the Poisson equation are obtained by the
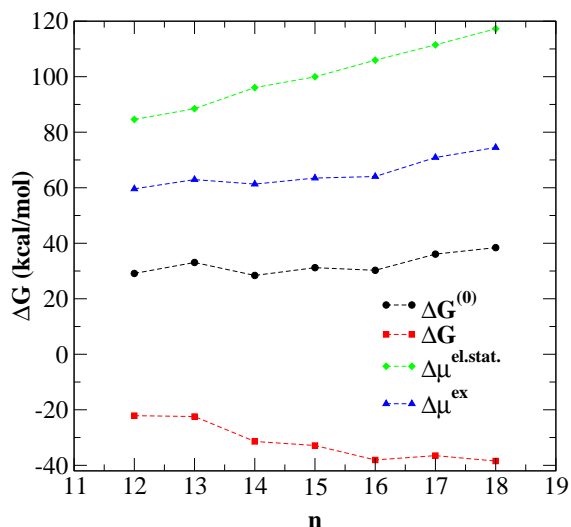
Figure 3.1. Free energies for hydrogen hydration in liquid water as a function of the number of inner shell water neighbors at $T = 298.15K$. The results labeled by $\Delta G^{(0)}$ (black circles) are the free energies estimated for the reaction $H_2 + nH_2O \rightleftharpoons H_2(H_2O)_n$ under standard ideal gas conditions, including $p = 1$ atm. The curve labeled by ΔG (red squares) incorporates the replacement free energy $-nRT\ ln\ 1354$ that adjusts the concentration of water molecules to the normal concentration of liquid water, $\rho_W = 1$ g/cm^3. The curve labeled by $\Delta\mu^{el}$ (green diamonds) depicts, $\Delta\mu^{el} = \mu^{el}_{H_2(H_2O)_n} - n\mu^{el}_{H_2O}$, the external solvent-cluster electrostatic contributions obtained from the standard dielectric model. The net excess chemical potential is labeled by $\Delta\mu^{ex}$ (blue triangles).

ChelpG method.[42] The atomic radii set is taken from Ref. [43]. The radius of the water molecule used to create the solvent exclusion grid is set to 1.4 Å. The Poisson equation is solved by utilizing the finite-difference method of the Adaptive Poisson-Boltzmann Solver (APBS) package,[44] with a minimum grid spacing of 0.1 Å, as described in detail in Ref. VARMA04A. The dielectric constant of the outer shell medium is set to 78.5 while the one of the inner shell is set to 1.0. The outer shell electrostatic contribution to the excess chemical potential, $\Delta\mu^{el} = \mu^{el}_{H_2(H_2O)_n} - n\mu^{el}_{H_2O}$, is shown in Fig. 3.1

3.2.2.3 Limitations and corrections

One of the advantages of the quasichemical approach to the studies of solvation processes, when compared to the more traditional methods, is that it circumvents the system size and CPU time limitations of computer simulation of complex molecular solutions. Moreover, partitioning of the region around the solute of interest into the domain of nearest neighbor interactions and the rest of the solution allows for the treatment of the inner domain chemical associations accurately by quantum chemistry methods while the outer domain, which is usually of secondary interest, can be treated in a more approximate fashion. Likewise, the quasichemical theory enables one to breakdown the net hydration free energy of the system of interest into individual contributions and as such allows one to gain better insight into hydration phenomena. In practical applications of the theory as utilized here, the inner domain is examined separately from the outer domain, and atomic motions in the inner domain that contribute to the thermodynamic properties of hydration are approximated by harmonic displacements from optimized geometries. The price that one pays for this divide-and-conquer approach implemented in the primitive fashion is introduction of approximations into the theory. Nevertheless, these approximations are amenable to improvements and corrections.

Harmonic approximations to the atomic motions within the clusters, implemented in the quantum chemistry calculations, are known to work well for the strongly bound systems (ionic type interactions) such as ion-water complexes with small coordination numbers (typically less than six).[30, 31, 34, 36] These systems exhibit stiff, high frequency intermolecular vibrational motions, that is, motions with very small excursions from the minimum energy geometry. In the case of the hydrophobic solvation of H_2 and Kr in liquid water, the structural studies have shown that the most probable coordination number is 16[17] and 18,[45, 46] respectively. A treatment of such relatively large, weakly bound complexes (with hydrogen-bond and hydrophobic interactions) within the harmonic approximation is unlikely to be adequate because of their large amplitude intermolecular vibrations.

We assess the effect of anharmonicity to the hydrogen hydration free energy in the following way. The earlier structural[17] and present thermodynamic studies carried out by the classical MC simulations (see Sec. 3.3.1) suggest that the implemented SPC/E classical force field and 3-site charge H_2 model[15, 17] adequately describe the interactions between water-water and H_2-water molecules. Thus the minimum energy geometries of the $H_2(H_2O)_n$ clusters obtained by electronic structure calculations (see Sec. 3.2.2.1) are used as the starting geometries for the energy minimization of the same clusters using intermolecular interactions between the cluster monomers modeled by the classical SPC/E force field and 3-site charge H_2 model.[15, 17] The normal mode (Hessian) analysis[47] is performed on the resulting minimum energy geometries and harmonic vibrational frequencies of the clusters are obtained, thus providing a determination of the free energy changes for the chemical reactions in Eq. (3.6) within the harmonic approximation. The harmonic free energy changes are listed in Table 3.2.

Table 3.2. Anharmonic (ΔG_{anharm}) and harmonic (ΔG_{harm}) free energy changes for the different cluster sizes in the inner shell and the corresponding estimate of the anharmonic contribution (δG) to the hydrogen hydration free energy. The numerical values are obtained by the GCMC technique in conjunction with the histogram method. All values are given in kcal/mol.

$H_2(H_2O)_n$	ΔG_{anharm}	ΔG_{harm}	δG
12	-77.3	-59.4	17.9
13	-84.4	-73.6	10.8
14	-91.6	-75.7	15.9
15	-99.0	-79.8	19.2
16	-106.5	-90.2	16.3
17	-113.7	-91.6	22.1
18	-121.2	-101.3	19.9

Anharmonic contributions[47] to the excess chemical potential are assessed by implementing the grand canonical Monte Carlo (GCMC) technique[25, 20] combined with the histogram method.[20, 48] The intermolecular interactions are modeled with the same SPC/E force field and 3-site charge H_2 model (see Table 3.1) that were utilized in the Gibbs Monte Carlo simulations (see Sec. 3.2.1). The relative free energy required to form water clusters of a given size around the hydrogen molecule is related to their respective probability of occurrence,

$$\Delta G(n) = -RT \, ln\frac{p_n}{p_{(n=0)}}, \tag{3.8}$$

where p_n is the probability that n water molecules surround the hydrogen molecule. In GCMC simulations a new microstate is generated by a displacement, rotation, and creation or destruction of a water molecule while the hydrogen molecule is held fixed. Water molecules are only allowed to occupy a sphere of radius 4.96 Å around the center of mass of the hydrogen molecule. The microstate thus generated is accepted or rejected so that the limiting distribution of the resulting microstates corresponds to the grand canonical ensemble distribution. Simulations are carried out at a temperature of 298.15 K, and excess chemical potential of 6.9 kcal/mol[49] for the range or window of water cluster sizes, where each window contains six water clusters of different size in an ascending order. Thus, window 1 consists of $n \in [0,5]$, window 2 of $n \in [3,8]$, window 3 of $n \in [6,11]$, ... , window 8 of $n \in [21,26]$. A histogram of the probability of occurrence for a given size of the water cluster is calculated within each window and the corresponding relative free energy of formation of the cluster is estimated from Eq. (3.8). The resulting free energy histograms are combined together using a simple weighted histogram analysis.[20] The final anharmonic free energies are obtained by subtracting the excess chemical potential of $n \times 6.9$ kcal/mol

from the histogram free energies and are shown in Fig. 3.2. Numerical values of the anharmonic free energy changes for the size of clusters in the range from $n = 12$ to $n = 18$ are listed in Table 3.2. The effect of anharmonicity to the hydrogen hydration free energy is obtained by subtracting the "anharmonic" free energy from the "harmonic" free energy, $\delta G = \Delta G_{harm} - \Delta G_{anharm}$.
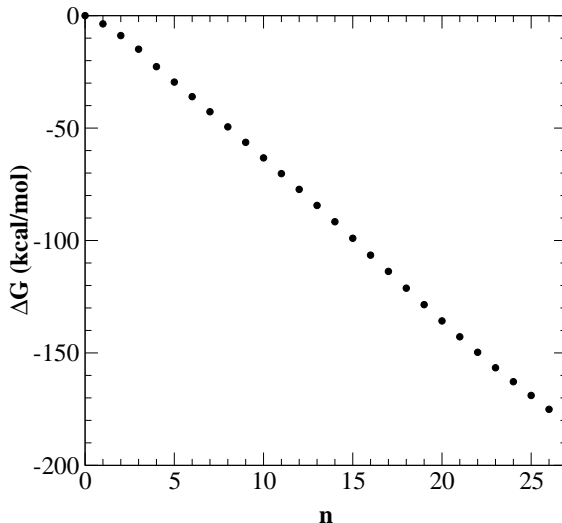
Figure 3.2. Free energy of formation of n water molecules around the hydrogen molecule obtained by GCMC in conjunction with the histogram method.

The explicit solvent contribution to the electrostatic interaction between the clusters in the inner shell and explicit water in the outer shell is determined by the thermodynamic integration method.[20] The electrostatic contribution to the hydrogen hydration free energy is given by[50]

$$\mu^{el} = \int_0^1 d\lambda \, \langle V \rangle_\lambda, \tag{3.9}$$

where λ is the coupling parameter and $\langle V \rangle_\lambda$ is the ensemble averaged potential present on the $H_2(H_2O)_n$ complex for a particular charge state λ. The estimate of the above integral is obtained by Gauss-Legendre quadrature.[51, 50] We used the two-point formula

$$\mu^{el} \approx \frac{1}{2} \left(\langle V \rangle_{\lambda_+} + \langle V \rangle_{\lambda_-} \right), \tag{3.10}$$

where $\lambda_\pm = (1/2 \pm 1/\sqrt{12})$. The electrostatic interaction is determined by allowing the inner shell clusters to move while interacting with the external water solvent. Implementation of the six point Gauss-Legendre quadrature[51] for the $H_2(H_2O)_{16}$ complex

changed the value of μ^{el} only modestly, by -1.7 kcal/mol. We report the results for $\Delta\mu^{el} = \mu^{el}_{H_2(H_2O)_n} - n\mu^{el}_{H_2O}$ obtained by the two-point quadrature formula and they are listed in Table 3.3. The value $\mu^{el}_{H_2O} = -6.5$ kcal/mol was taken from Ref. [57] and $\mu^{el}_{H_2(H_2O)_n} \equiv \mu^{el}$.

The B3LYP hybrid density functional utilized to evaluate minimum energy structures of hydrogen-water complexes, $H_2(H_2O)_n$, does not account for the inner shell dispersion H_2-H_2O interactions. Therefore we implement the MP2 level of theory to treat the dispersion interactions between a H_2-H_2O pair, which yields a correction value of -0.16 kcal/mol for the energy of each H_2-H_2O pair.

An additional approximate correction that we take into account and include in the net excess chemical potential is due to a residual entropy associated with multiple orientational configurations of water. Assuming an ideal tetrahedral coordination for each water molecule, the residual entropy is $S/k \approx ln(3/2)^n$,[52] where n is the number of water molecules in the $H_2(H_2O)_n$ complex.

3.2.3 Quasichemical theory: "An inverse approach"

A slightly different and complementary approach to evaluating the free energy of hydration is based on the estimate of the chemical (inner) and outer sphere contributions directly from molecular simulations. The advantage in analyzing data from a molecular simulation is the automatic inclusion of anharmonic effects in the thermal energies. Equation (3.5) can be rewritten as follows[53]

$$\mu^{ex}_{H_2} = RT\ ln\ x_0 - RT\ ln\ p_0 + \mu^{el} + \mu^{vdW}_{out}, \tag{3.11}$$

where the outer sphere contribution consists of the last three terms. The second term, $\mu^{pac} = -RT\ ln\ p_0$, represents the molecular packing. This term corresponds to the free energy required to form a cavity in the solvent with the same size and shape as the inner shell, where p_0 is the probability of finding the cavity of a given size. The last two terms represent the interaction part of the outer shell contribution, that is, interactions of the solute in an empty inner shell with the outer shell solvent molecules. The μ^{el} term is an electrostatic one while the μ^{vdW}_{out} term represents a dispersion interaction contribution to the excess free energy.

The probability x_0 (or the quantity $ln\ x_0$) is estimated from the coordination number distribution determined earlier[17] by the classical Monte Carlo simulations. We utilize the polynomial interpolation/extrapolation scheme[54] to fit an interpolating polynomial to the coordination number distribution data (see Fig. 3.3) and evaluate the resulting polynomial at the coordination number $n = 0$.

The probability of p_0 is estimated as follows. Ten thousand configurations stored during the Monte Carlo simulations[17] performed earlier are analyzed. For each configuration,

48
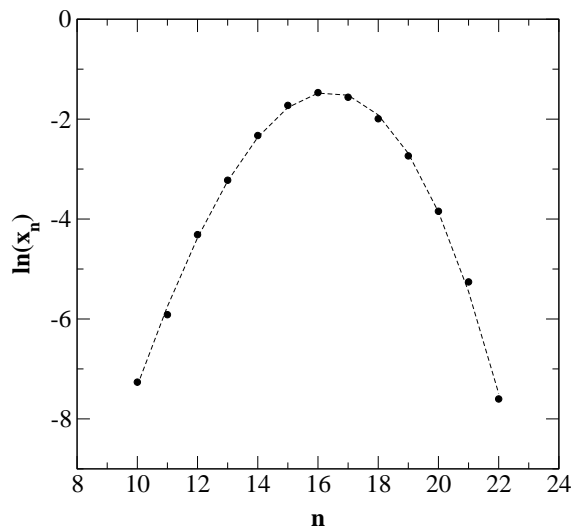
Figure 3.3. The coordination number distribution determined in the earlier MC simulations[17] is depicted by the solid circles while an interpolating polynomial is represented by a dashed line.

a simulation box is divided into a cubic grid with the spacing between grid points varying from 1 to 0.5 Å depending on the size of the seeking cavity (a larger cavity requires a finer grid). Around each grid point a sphere of radius R_c is formed and the number of molecules present in the given volume is counted. The grid points associated with unoccupied volumes are counted as cavities. The probability p_0 is yielded by dividing the number of found cavities by the total number of grid points. The probability p_0 of finding a cavity with a radius of the inner shell, $R_c = 4.96$ Å, is extremely small and could not be found directly. Thus, we calculate p_0 as a function of the radius of a cavity in the range from 0.2 to 4.0 Å. The resulting data points are fitted to an interpolating polynomial (see Fig. 3.4) by utilizing an interpolation/extrapolation scheme[54] and the resulting polynomial is evaluated at $R_c = 4.96$ Å.

The electrostatic interaction term, μ^{el}, is modeled within a dielectric continuum approach by utilizing the APBS package.[44] A quadrupole moment of the hydrogen molecule is constructed from two sets of charges that are placed on the hydrogen nuclei and the center of mass of the hydrogen molecule. The first set of charges is taken from Table 3.1 and the second one is obtained from the electronic structure calculations[40] of the hydrogen molecule.

In order to estimate the outer shell dispersion contribution term, μ_{out}^{vdW}, we assume that the interaction between the solute (H_2) and outer shell solvent (water) is of the form $-4\varepsilon\sigma^6/r^6$, where the solvent is treated as a uniform medium.[45] Then, the outer shell dispersion contribution can be obtained analytically from the following integral[55, 25]
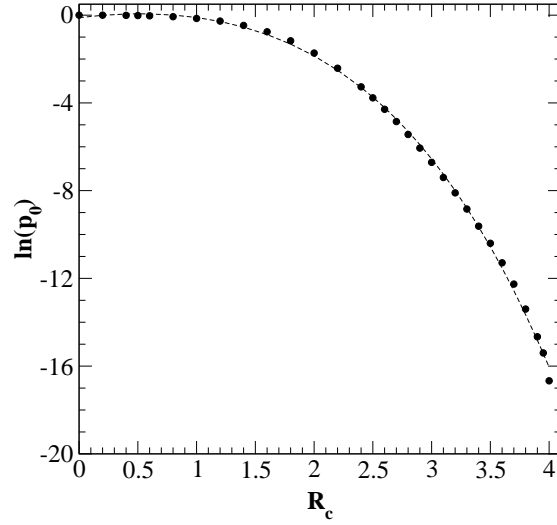
Figure 3.4. The natural logarithm of a probability of observing a cavity of a given size in liquid water. Solid circles represent the calculated data while an interpolation polynomial is depicted by a dashed line.

$4\pi\rho_w \int_{R_c}^{\infty} dr\, r^2(-4)\varepsilon\sigma^6/r^6$ which yields

$$\mu_{out}^{vdW} = -\frac{16\pi\varepsilon}{3}\left(\frac{\sigma}{R_c}\right)^3 \rho_w\sigma^3, \tag{3.12}$$

where $\varepsilon = 0.103$ kcal/mol and $\sigma = 3.102$ Å are the Lennard-Jones parameters for H_2-water interactions (see Table 3.1), $R_c = 4.96$ Å is the inner shell radius and $\rho_w = N_w/L^3$ is the number density of water ($N_w = 136$ is a number of water molecules in the simulation box; $L = 16.14$ Å is the average length of the simulation box).

3.3 Results and discussion

In this section, we present the results of MC simulations carried out on hydrogen molecules solvated in water as well the results obtained by the complementary quasichemical theory. Details about the calculations were given in Section 3.2.

3.3.1 Monte Carlo

Monte Carlo simulations carried out in the NVT- and NpT-Gibbs ensembles yield the hydrogen hydration free energy of 2.20 ± 0.22 and 2.09 ± 0.26 kcal/mol, respectively, which are in excellent agreement with the experimental value of 2.34 kcal/mol.[56] The error bars correspond to two standard deviations from the mean. Such an excellent agreement between the calculated and experimental values of the hydration free energy suggests that the implemented classical force field provides a good description of intermolecular interactions between hydrogen and water molecules.

3.3.2 Quasichemical theory:"An inverse approach"

The numerical value of the molecular packing contribution, $-RT \ln p_0$, to the free energy of hydrogen hydration for a cavity of radius 4.96 Å is 18.94 kcal/mol. This value nearly balances the inner shell chemical association contribution, $RT \ln x_0 = -17.59$ kcal/mol. Similar, nearly balanced inner shell chemical effects and outer shell molecular packing contributions were observed in the thermodynamic studies of liquid water.[57, 53]

The outer shell electrostatic interaction term, μ^{el}, which accounts for electrostatic interactions between the solute in an empty inner shell and the solvent molecules in the outer shell (which were treated as a dielectric continuum) exhibits negligible values of $-6.2 \cdot 10^{-4}$ kcal/mol and $-1.3 \cdot 10^{-3}$ kcal/mol. The former value is obtained using the set of charges from Table 3.1 and the latter is estimated by using the set of charges yielded by the Gaussian package (see Section 3.2.3 for details). Such a small contribution of the electrostatic term to the free energy of hydrogen solvation is consistent with the nonpolar nature of the hydrogen molecule.

The outer shell dispersion interaction, μ^{vdW}, between the solute in an empty inner shell and a dielectric continuum in the outer shell is estimated from Eq. (3.12) and yields the numerical value of -0.4 kcal/mol (see Section 3.2.3 for details). By substituting these estimated numerical values in Eq. (3.11), we obtain the hydrogen hydration free energy $\mu_{H_2}^{ex} = 0.95$ kcal/mol, a value which is in good agreement with the experimental value of 2.34 kcal/mol.

3.3.3 Quasichemical theory:"A direct approach"

Figure 3.1 shows the net excess free energy of hydrogen hydration and its individual terms. From Fig. 3.1 it is not possible to determine reliably the most probable coordination number of the hydrogen molecule in liquid water. The most probable coordination number is the one associated with the lowest excess free energy. The excess free energies for the various clusters lie within 4.5 kcal/mol of each other, with the exception of the larger clusters $(n = 17, 18)$. In addition, the absolute values of free energies are of the order of

Table 3.3. The hydrogen hydration free energy $\Delta\mu^{ex}$ and its individual terms: $\Delta G^{(0)}$—the free energy change for ideal gas phase chemical reactions in Eq. (4.1); $\Delta G = \Delta G^{(0)} - nRT \ \ln \ 1354$—the free energy change accounting for the actual density of water; $\Delta\mu^{el}$— the electrostatic interaction between clusters in the inner shell and the explicit solvent in the outer shell; δG— the anharmonic contribution to the free energy; $\mu^* = nRT \ \ln(3/2)$—contribution due to multiple orientational configurations of water; μ_{out}^{vdW}— the outer shell dispersion contribution; μ_{in}^{vdW}— the inner shell dispersion contribution; $\mu^{pac} = -RT \ \ln \ p_0$— the molecular packing contribution. All values are given in kcal/mol.

$H_2(H_2O)_n$	$\Delta G^{(0)}$	ΔG	$\Delta\mu^{el}$	δG	μ^*	μ_{out}^{vdW}	μ_{in}^{vdW}	μ^{pac}	$\Delta\mu^{ex}$
12	29.1	-22.1	38.2	17.9	2.9	-0.4	-1.9	18.9	11.9
13	33.1	-22.4	42.1	10.8	3.1	-0.4	-2.1	18.9	22.2
14	28.4	-31.4	45.7	15.9	3.4	-0.4	-2.2	18.9	11.3
15	31.2	-32.9	51.4	19.2	3.6	-0.4	-2.4	18.9	11.9
16	30.3	-38.1	55.2	16.3	3.8	-0.4	-2.6	18.9	13.0
17	36.1	-36.5	59.7	22.2	4.1	-0.4	-2.7	18.9	12.8
18	38.4	-38.5	65.0	19.9	4.3	-0.4	-2.9	18.9	17.9

≈ 60 kcal/mol, which is a value almost greater by a factor of 30 than the experimental value. It should be noted that the excess free energies include the correction $\mu^* = nRT \ \ln(3/2)$, but do not include the inner shell dispersion, outer shell dispersion and packing contribution correction with the numerical values of $-n \times 0.16$, -0.4 and 18.94 kcal/mol, respectively. Clearly, the dispersion corrections are too small to make an appreciable change in the excess free energy while the packing contribution, being positive, makes the agreement between the final excess free energy and experimental value even worse. A large discrepancy between the calculated and experimental hydration free energy is primarily attributed to two approximations:

1. treatment of the solvation complexes within the harmonic approximation and

2. treatment of the outer shell solvent as a dielectric continuum medium.

The estimate of the anharmonic correction, δG, to the harmonic approximation utilized in the quasichemical theory is given in Table 3.3 for each $H_2(H_2O)_n$ complex. The anharmonic effects are in the range from 11 to 22 kcal/mol depending on the size of the complex, and further stabilize each complex.

The explicit solvent electrostatic contribution to the net free energy is approximately 50 kcal/mol smaller (more favorable) than its dielectric continuum counterpart. That is to

say, the dielectric continuum model overestimates the electrostatic interactions between the clusters in the inner shell and outer shell solvent by approximately 50 kcal/mol. For example, the net free energy of the $H_2(H_2O)_{16}$ complex that also includes the molecular packing contribution is 80.03 kcal/mol. After taking into account the complex's corresponding anharmonic and explicit solvent (favorable) corrections of 16.31 and 50.76 kcal/mol, respectively, the net free energy amounts to 13.0 kcal/mol, a value within 10.7 kcal/mol of the experimental value. The net free energy is obtained from the following expression: $\Delta\mu^{ex} = \Delta G^{(0)} - nRT \ln 1354 - \delta G - \mu^* + \mu_{in}^{vdW} + \Delta\mu^{el} + \mu_{out}^{vdW} + \mu^{pac}$. The first five terms can be noted as the inner shell while the last three terms as the outer shell contributions to the hydration free energy. As with the "indirect" approach, the inner and outer shell contributions almost cancel each other out and yield a result in reasonably good agreement with the experimental result when compared to the uncorrected excess chemical potential(s) shown in Fig. 3.1.

3.4 Conclusions

In the present work, we investigate the thermodynamic properties of hydrogen hydration in liquid water by employing the quasichemical theory and Monte Carlo simulations combined with the SPC/E classical force field and a 3-site charge H_2 model.

The hydrogen hydration free energy of 2.20 ± 0.22 and 2.09 ± 0.26 kcal/mol obtained by the Monte Carlo simulations carried out in the NVT- and NpT-Gibbs ensembles, respectively, are in excellent agreement with the experimentally measured value of 2.34 kcal/mol.[56] The results indicate that the classical force field employed in this work provides a good description of the intermolecular interactions between water-water and water-hydrogen molecules. Similarly, recent structural studies[17] of hydrogen hydration in liquid water have shown that this classical force field produces the structural properties equivalent to those produced by *ab initio* derived forces. Thus, the classical force field employed in the current work seems to be adequate for the studies of structural and thermal properties of hydrogen hydration in both liquid[17] and clathrate phases.[15]

Quasichemical approaches provide complementary insight to the thermodynamic properties of aqueous solutions, in general, and to hydrophobic hydration phenomena, in particular. Although formally exact, their direct practical application utilizes a set of simplifying approximations. The approximations, such as harmonic atomic motions and a treatment of the solvent as a dielectric continuum medium, have proven to be suitable for studies of ion hydration phenomena[30, 31, 32, 33, 34, 35, 36] as well as in studying the selectivity of some biological ion channels.[37] These systems are relatively strongly bound and the aforementioned approximations are well suited for their treatment. In contrast, the hydrophobic systems, such as hydrogen solvated in liquid water, are relatively weakly bound and known to exhibit large amplitude motions for which the harmonic approximation breaks down.

Anharmonic effects, for example, contribute significantly (16 kcal/mol) to the net hydration free energy of hydrogen hydration for the $H_2(H_2O)_{16}$ cluster, the most probable coordination structure[17] for hydrogen in liquid water. Corrections to the dielectric continuum model are even greater than those for anharmonicity. For the same 16-coordinated hydrogen water cluster, the correction for explicit solvent is of the order of 51 kcal/mol, which amounts to approximately 3.2 kcal/mol per water molecule. Differences in contributions to the hydration free energy from the external solvent occur because a dielectric model approximation keeps the inner shell clusters fixed in their minimum energy configurations while interacting with the external continuum solvent medium. In contrast, explicit solvent calculations allow the inner shell clusters to move while interacting with the external explicit water solvent.

Although the "direct" quasichemical approach provides a natural description of the statistical thermodynamics of hydrophobic hydration phenomena and also enables breakdown of the net hydration free energy into individual components for additional insight into hydration, care must be exercised when applying simplifying approximations. Since anharmonic effects and explicit solvent play an important role in the determination of the hydrophobic hydration free energy, corrections, as carried out here, should be applied to account for them. In some cases, small relative errors in the outer and inner shell terms, large contributions that nearly balance each other, may cause errors in the net hydration free energy and diminish agreement with the experimental results.

An "inverse" quasichemical approach yields the hydration free energy of approximately 1.0 kcal/mol, a numerical value which is in good agreement with experiment. Possible reasons for the small discrepancy with experiment include these: the outer dispersion interaction is obtained by using a dielectric model; both chemical association and molecular packing terms are obtained by an extrapolation procedure. The chemical and packing terms provide nearly cancelling contributions to the hydrogen hydration, an effect also seen in the hydration of water.[57, 53] This may suggest that the local structure of water around the hydrogen solute is only weakly perturbed from its bulk structure and thermodynamically resembles bulk water. In summary, we have found that the net free energy of hydrogen hydration results from a balance between chemical associations taking place within the first hydration shell and molecular packing of the solvent molecules around it.

References

[1] C. Tanford. *Protein Sci.*, 6:1358, 1997.

[2] W. Kauzmann. *Adv. Protein Chem.*, 14:1, 1958.

[3] K. A. Dill. *Biochemistry*, 29:7133, 1990.

[4] C. Tanford. *Science*, 200:1012, 1978.

[5] I. Chatti, A. Delahaye, L. Fournaison, and J.-P. Petitet. *Energy Convers. Manage.*, 46:1333, 2005.

[6] E. Suess, G. Bohrmann, J. Greinert, and E. Lausch. *Sci. Am.*, 281:76, 1999.

[7] W. L. Mao and H.-K. Mao. *Proc. Natl. Acad. Sci. U.S.A.*, 101:708, 2004.

[8] E. D. Sloan. *Clathrate Hydrates of Natural Gases*. Marcel Dekker Inc., New York, 2nd edition, 1998.

[9] Y. A. Dyadin, E. D. Larinov, A. Y. Manakov, F. V. Zhurko, E. Y. Aladko, T. V. Mikina, and V. Y. Komarov. *Mendeleev Commun.*, 5:209, 1999.

[10] W. L. Mao, H.-K. Mao, A. F. Goncharov, V. V. Struzhkin, Q. Guo, J. Hu, J. Shu, R. J. Hemley, M. Somayazulu, and Y. Zhao. *Science*, 297:2247, 2002.

[11] L. J. Florusse, C. J. Peters, J. Schoonman, K. C. Hester, C. A. Koh, S. F. Dec, K. N. Marsh, and E. D. Sloan. *Science*, 306:469, 2004.

[12] K. C. Hester, T. A. Strobel, E. D. Sloan, C. A. Koh, A. Huq, and A. J. Schultz. *J. Phys. Chem. B*, 110:14024, 2006.

[13] S. Patchkovskii and J. S. Tse. *Proc. Natl. Acad. Sci. U.S.A.*, 100:14645, 2003.

[14] K. A. Lokshin, Y. Zhao, D. He, W. L. Mao, H.-K. Mao, R. J. Hemley, M. V. Lobanov, and M. Greenblatt. *Phys. Rev. Lett.*, 93:125503, 2004.

[15] S. Alavi, J. A. Ripmeester, and D. D. Klug. *J. Chem. Phys.*, 123:024507, 2005.

[16] J. S. Clawson, D. Sabo, S. B. Rempe, K. Leung, R. T. Cygan, and T. M. Alam. Ab initio study of hydrogen occupancy in hydrogen clathrate hydrates. to be published.

[17] D. Sabo, S. B. Rempe, J. A. Greathouse, and M. G. Martin. *Mol. Sim.*, 32:269, 2006.

[18] see http://towhee.sourceforge.net.

[19] A. Z. Panagiotopoulos. *Mol. Phys.*, 61:813, 1987.

[20] D. Frenkel and B. Smit. *Understanding Molecular Simulation*. Academic Press, San Diego, 2002.

[21] A. Z. Panagiotopoulos, N. Quirke, M. Stapleton, and D. J. Tildesley. *Mol. Phys.*, 63:527, 1988.

[22] M. G. Martin and J. I. Siepmann. *J. Phys. Chem. B*, 103:4508, 1999.

[23] H. J. C. Berendsen, J. R. Grigera, and T. P. Straatsma. *J. Phys. Chem.*, 91:6269, 1987.

[24] J. O. Hirschfelder, C. F. Curtiss, and R. B. Bird. *Molecular Theory of Gases and Liquids*. Wiley, New York, 1954. p.168.

[25] M. P. Allen and D. J. Tildesley. *Computer Simulation of Liquids*. Oxford University Press, Oxford, 1996.

[26] By a direct approach, we mean a 'building up cluster' approach in which the solute molecule of interest is successively solvated by an increasing number of surrounding solvent molecules.

[27] L. R. Pratt and S. B. Rempe. Quasi-chemical theory and implict solvent models for simulations. In L. R. Pratt and G. Hummer, editors, *Simulation and Theory of Electrostatic Interactions in Solution*, volume 492, page 172. AIP Conf. Proc., New York, 1999.

[28] M. E. Paulaitis and L. R. Pratt. *Adv. Prot. Chem.*, 62:283, 2002.

[29] T. L. Beck, M. E. Paulaitis, and L. R. Pratt. *The potential distribution theorem and models of molecular solutions*. Cambridge University Press, Cambridge, 2006.

[30] S. B. Rempe, L. R. Pratt, G. Hummer, J. D. Kress, R. L. Martin, and A. Redondo. *J. Am. Chem. Soc.*, 122:966, 2000.

[31] S. B. Rempe and L. R. Pratt. *Fluid Phase Equilib.*, 183-184:121, 2001.

[32] D. Asthagiri, L. R. Pratt, and H. S. Ashbaugh. *J. Chem. Phys.*, 119:2702, 2003.

[33] D. Asthagiri and L. R. Pratt. *Chem. Phys. Lett.*, 371:613, 2003.

[34] S. B. Rempe, D. Asthagiri, and L. R. Pratt. *Phys. Chem. Chem. Phys.*, 6:1966, 2004.

[35] D. Asthagiri, L. R. Pratt, and J. D. Kress. *Proc. Natl. Acad. Sci. U.S.A.*, 102:6704, 2005.

[36] S. Varma and S. B. Rempe. *Biophys. Chem.*, 124:192, 2006.

[37] S. Varma and S. B. Rempe. Tuning ion coordination preferences to enable selective permeation. http://arXiv.org/abs/physics/0608180.

[38] H. P. Hansen and I. R. McDonald. *Theory of Simple Liquids*. Academic Press, New York, 1986.

[39] B. Widom. *J. Phys. Chem.*, 86:869, 1982.

[40] M. J. Frisch, et al. Gaussian 98, 1998. revision A.2; Gaussian, Inc., Pittsburgh, PA.

[41] R. L. Martin, P. J. Hay, and L. R. Pratt. *J. Phys. Chem. A*, 102:3565, 1998.

[42] C. M. Breneman and K. B. Wiberg. *J. Comput. Chem.*, 11:361, 1990.

[43] E. V. Stefanovic and T. N. Truong. *Chem. Phys. Lett.*, 244:65, 1995.

[44] N. A. Baker, D. Sept, S. Joseph, M. J. Holst, and J. A. McCammon. *Proc. Natl. Acad. Sci. U.S.A.*, 98:10037, 2001.

[45] H. S. Ashbaugh, D. Asthagiri, L. R. Pratt, and S. B. Rempe. *Biophys. Chem.*, 105:323, 2003.

[46] R. A. LaViolette, K. L. Copeland, and L. R. Pratt. *J. Phys. Chem. A*, 107:11267, 2003.

[47] S. B. Rempe, K. Leung, and S. Varma. unpublished results.

[48] D. P. Landau and K. Binder. *A Guide to Monte Carlo Simulations in Statistical Physics*. Cambride University Press, Cambridge, 2002.

[49] J. C. Shelley and G. N. Patey. *J. Chem. Phys.*, 102:7656, 1995.

[50] G. Hummer and A. Szabo. *J. Chem. Phys.*, 105:2004, 1996.

[51] M. Abramowitz and I. A. Stegun. *Handbook of Mathematical Functions*. Dover, New York, 1965.

[52] L. Pauling. *J. Am. Chem. Soc.*, 57:2680, 1935.

[53] A. Paliwal, D. Asthagiri, L. R. Pratt, H. S. Ashbaugh, and M. E. Paulaitis. *J. Chem. Phys.*, 124:224502, 2006.

[54] W. H. Press, S. A. Teukolsky, W. T. Vetterling, and B. P. Flannery. *Numerical Recipes*. Cambridge University Press, Cambridge, 2nd edition, 1992.

[55] D. A. McQuarrie. *Statistical Mechanics*. Harper & Row, New York, 1976.

[56] C. L. Young, editor. *Hydrogen and deuterium (Solubility data series)*, volume 5/6. Pergamon Press, Oxford, 1981.

[57] D. Asthagiri, L. R. Pratt, and J. D. Kress. *Phys. Rev. E*, 68:041505, 2003.

Chapter 4

Quantum chemical study of hydrogen occupancy in clathrate hydrate cages

4.1   Introduction

Clathrate hydrates belong to a group of inclusion solid state compounds in which hydrogen-bonded water molecules form host polyhedra cages that trap hydrophobic guest molecules.[1] The thermodynamic stability of the clathrate hydrate lattice depends on both the identity of the guest molecule(s) and specific conditions of temperature and pressure. While methane clathrate hydrates have long been known to exist in arctic soils and beneath the sea floor, recent experimental results have demonstrated the possibility of synthesizing a whole new class of clathrate hydrates that trap hydrogen gas.[2, 3] Interest in hydrogen clathrate hydrates centers around their potential use as an alternative material for hydrogen storage.[4]

Experimental investigations show that hydrogen clathrate hydrates crystallize by forming the so-called sII type cubic structure. A unit cell of the sII clathrate consists of 16 "small" dodecahedral cages, polyhedrons with 12 pentagonal faces (5^{12}) made up of 20 water molecules, and 8 "large" hexakaidecahedral cages, polyhedrons with 12 pentagonal and 4 hexagonal faces ($5^{12}6^4$) made up of 28 water molecules.[5, 6] In order to be a good candidate for a storage medium, clathrate hydrates must uptake a substantial amount of hydrogen into the cages of the clathrate structure.

Studies to identify the hydrogen occupancy of pure hydrogen clathrate cages have been inconclusive. Initial experiments[3] and theoretical studies based on quantum mechanically derived forces[5, 7] have reported double (quadruple) occupancy of the small (large) cages, while more recent experiments[8] and theoretical studies based on classical force fields[9] have instead found only single hydrogen molecule occupancy in the small cages. Double occupancy by hydrogen molecules in the small cages accompanied by quadruple occupancy in the large cages leads to a 5.3 weight per cent mass storage capacity, which meets the 2006 DOE target for hydrogen fuel storage. Single occupancy in the small cages as illustrated in

Figure 4.1, however, reduces the mass ratio to only 3.9 weight per cent. To evaluate these materials for their potential to store hydrogen, the distribution of hydrogen in the clathrate hydrate cages must be unambiguously determined.

In the present work, we examine the most probable hydrogen occupancy in isolated "small" and "large" hydrogen clathrate cages by employing methods based on a quantum mechanical description of the intermolecular interactions. In Sec. 4.2 we describe the computational methods employed to calculate hydrogen occupancy in the isolated hydrogen clathrate hydrate cages. In Sec. 4.3 we present the results of our calculations. Finally, we summarize our findings in Sec. 4.4.

4.2   Computational Details

The oxygen positions of the water cages are obtained from an X-ray structure for a type-II hydrated clathrate.[10] The hydrogen bonding network, not available from the scattering data, is generated using classical force field simulations.[11] Lattice constants for a single unit cell are then optimized using the Vienna *ab initio* simulation package (VASP)[12, 13] based on a generalized gradient approximation (GGA) of the Perdew-Wang (PW91) density functional[14, 15, 16, 17, 18] using gamma-point Brillouin sampling and a 400 eV cut-off for the plane-wave expansion.

Multiple samples of two types of cages, one small and one large, are extracted from the optimized type II clathrate unit cell and reaction energy calculations are performed for various cage occupations at a temperature of 0 K and ambient and experimental pressures of hydrogen gas. The energy calculations employ the Gaussian suite of programs.[19] Hydrogen molecule occupancies between 1 and 3 and between 1 and 5 are considered for the small and large cages, respectively. In all cases, the guest H_2 molecules are fully optimized in these fixed cages using a restricted Becke's three-parameter hybrid functional[20] with the Lee, Yang, and Parr correlation functional[21] (rB3LYP) and the 6-311G[22, 23] basis set. For each optimization, several starting positions are considered to help ensure that a global minimum has been reached. Single point energy calculations are performed using the second-order Möller-Plesset (MP2)[24] level of theory to incorporate dispersive interactions due to eletron correlation. The minimum basis set required to converge the reaction energy calculations is determined in a study using the small cage with increasingly larger basis sets: $3-21G$,[25, 26, 27, 28, 29, 30] $6-311G$, $6-311G^*$, $6-311G^{**}$, $6-311+G^*$ to $6-311++G^{**}$. The large cage reaction energies are calculated using this same minimum basis set.

The reaction energies for incorporation of hydrogen molecules in the type-II clathrate cages are calculated by using the following reaction:
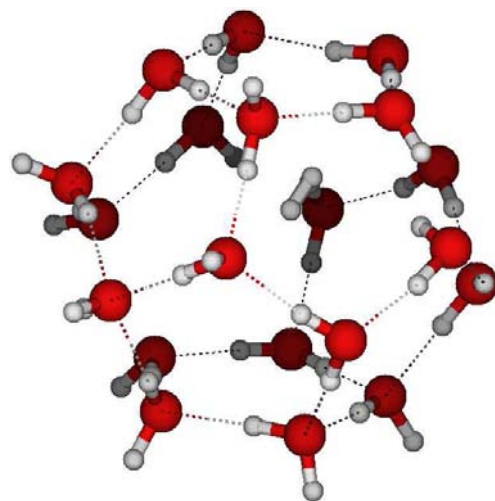
$$nH_2 + Cage \rightarrow nH_2@Cage \tag{4.1}$$

(a)
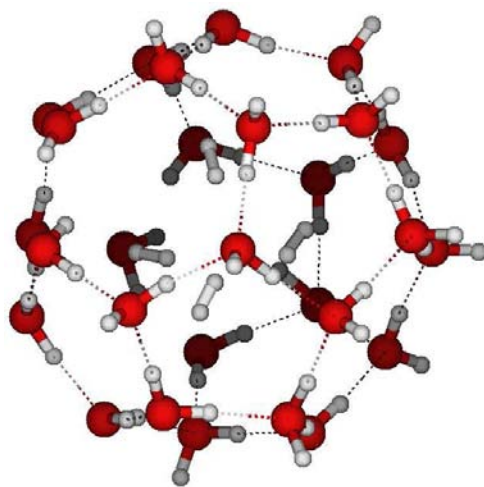
(b)

Figure 4.1. The most probable occupancy of the H$_2$ guest molecules in the sII clathrate cages. (a) Singly-occupied small cage. (b) Four-fold occupied large cage. The hydrogen bonding networks of the two cages are shown by dotted lines.

and

$$\Delta E = E(nH_2@Cage) - [E(nH2) + E(Cage)]$$
$$-nRT \; ln(P/P_0), \qquad\qquad (4.2)$$

where n is the number of guest H_2 molecules, $E(Cage)$ is the energy of the rigid isolated cage, and $E(nH_2)$ is the energy of n optimized free H_2 molecules. The pressure of hydrogen gas relative to ambient pressures is given by the ratio P/P_0, T gives the temperature and R is the gas constant.

Free volume calculations for the type-II hydrate are performed using the algorithm of Voorintholt et al.[31] and the Materials Studio software package (Accelrys, Inc., San Diego). Van der Waal radii for water molecule atoms are taken from the solvent-based optimizations of Stefanovich and Truong.[32] The guest hydrogen molecules are modeled by two connected spheres of radius 1.0 Å.

4.3 Results and discussion

4.3.1 Unit cell optimization

The optimized lattice constant is 16.945 Å, slightly smaller than the experimental value of 17.31 Å near room temperature. The binding energy per water molecule, not including zero point correction, is 0.71 eV. This value is very similar to the 0.72 eV binding energy for ice Ih predicted by Feibelman.[33] Thus, despite the more open structure of the clathrate hydrate compared to ice Ih, they are very similar in stability, which underscores the viability of clathrate hydrate structures. The optimized O-H bond lengths are 1.015 ± 0.006 Å, which are longer than the O-D bond length in ice Ih (0.975 Å), but well within typical O-H bond lengths.

4.3.2 Structure of H_2 inside isolated cages

The structural information for the optimized H_2 molecules inside the isolated clathrate cages is listed in Table 4.1 including the H-H bond lengths, the distances from the center of mass of the cage (cm) to the center of mass of the H_2 molecule (H_2^{cm}), the distance from the closest water oxygen (O*) to the center of mass of the H_2 molecule (H_2^{cm}), and the distance between the centers of mass of H_2 molecules. The optimized geometries of the guest hydrogen clusters found in this work are similar to the geometries described in the earlier quantum chemical work by Patchkovskii and Tse.[5]

The optimized H-H bond lengths are $\sim 1\%$ longer than the gas phase length of 0.741 Å, implying that the guest H_2 molecules inside the cages experience weak repulsive forces

Table 4.1. Structural properties of n H_2 optimized in rigid clathrate cages. Guest H_2 positions are fully optimized inside the rigid cages at the rB3LYP/$6-311$G level of density functional theory. [a]S indicates the small (D-5^{12}) cage and L indicates the large (H-$5^{12}6^4$) cage. [b]cm is the center of mass of the cage and H_2^{cm} is the center of mass of the H-H bond. [c]O* is the distance of nearest cage oxygen atom to the center of mass of the H_2 molecule.

Reaction [a]	Avg r(H-H) Å	Avg r(C-H_2^{cm}) [b] Å	Avg r(H_2^{cm}-O*) [c] Å	Avg r(H_2^{cm}-H_2^{cm}) Å
$1H_2+S= 1H_2@S$	0.746	0.78	3.02	NA
$2H_2+S= 2H_2@S$	0.742	1.26	2.70	2.51
$3H_2+S= 3H_2@S$	0.737	1.49	2.67	2.57
$1H_2+L= 1H_2@L$	0.747	1.74	2.91	NA
$2H_2+L= 2H_2@L$	0.744	1.65	3.20	3.18
$3H_2+L= 3H_2@L$	0.743	1.85	3.00	3.05
$4H_2+L= 4H_2@L$	0.743	1.86	2.92	3.01
$5H_2+L= 5H_2@L$	0.742	1.98	2.84	3.09

with the exception of the three-fold occupied small cage. At this occupation, the average H-H bond length decreases to 0.737 Å indicating a strong repulsive force between hydrogen molecules due to crowding inside the cage. When clusters of H_2 molecules are optimized outside of the cage, the H-H bond lengths are consistently 0.742 Å.

In order to accommodate multiple occupancies in the small cage, the distance between the H_2 molecules decreases by $15-18\%$ compared to the same occupancy inside the large cage (see Table 4.1). This result is consistent with the distances reported in molecular dynamics simulations (H_2^{cm}-H_2^{cm} distances of 3.0 Å and 2.65 Å for the large and small cages, respectively).[9] In addition, the distance between the H_2 molecules in the four-fold occupied large cage, 3.01 Å, closely reproduces the experimental D_2 distance value of 2.93 Å.[8] This decrease in the intermolecular distance is further evidence of the repulsive forces, which destabilize multiple occupancies in the small cage.

The major difference in H_2 geometry between this and the earlier quantum chemical results[5] are found with a single H_2 guest molecule in the small cage. Patchovskii and Tse[5] reported an energy minimum at 1.1 Å from the center of the cage, while the H_2 molecule is much closer to the center (0.78 Å) of the cage in this study. Two changes are made in this study: level of theory and the structure of the clathrate cage. Patchkovskii and Tse[5] used the $3-21$G(p) basis set and set O-H bond lengths to 1.0 Å. Using the optimized clathrate cages and the $3-21$G basis, the H_2 molecule position optimized to the same 1.1 Å minimum. However, the reaction energy calculated using this geometry is much higher. Therefore, we conclude that the 1.1 Å minimum is likely a consequence of the smaller basis set.
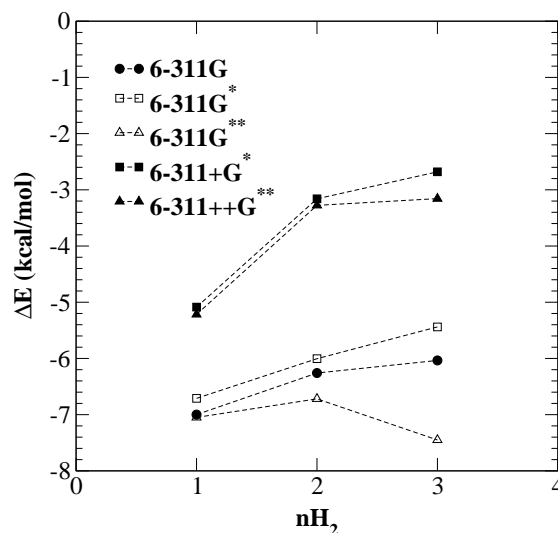
Figure 4.2. Reaction energies (ΔE) as a function of guest H_2 occupancy in the small cage at 2000 bar. All calculations are performed with MP2 level of theory. The basis set is given in the legend.

4.3.3 Quantum chemical reaction energies

Figure 4.2 shows the reaction energies for various H_2 occupancies inside the small cage at a pressure of 2000 bar and temperature of 0 K.

All calculations are carried out with the MP2 level of theory to incorporate weakly attractive dispersion interactions arising from electron correlation. The reaction energy converges at the $6-311+G^*$ basis set. At this level of theory, the reaction energy of the small cluster increases significantly after the first guest H_2 molecule has been added. Thus, the optimal occupancy of the small cage is one H_2 guest molecule. As is evident from Figure 4.3 this is not the case for the large cage. The reaction energy of this cage decreases when more than one H_2 molecule is placed inside the cage. At ambient pressure, the large cage favors a double occupancy (dashed line), while at the experimental pressure (2000 bar) the occupancy increases to four (solid line). Lokshin[8] noted similar changes in the occupancy of D_2 guest molecules in the clathrate II structure.

4.3.4 Available volume

The available volume inside the cage alone will restrict the occupancy. To estimate the free volume, a spherical probe of radius 1.4 Å is traced onto the hydrogen bonded network of
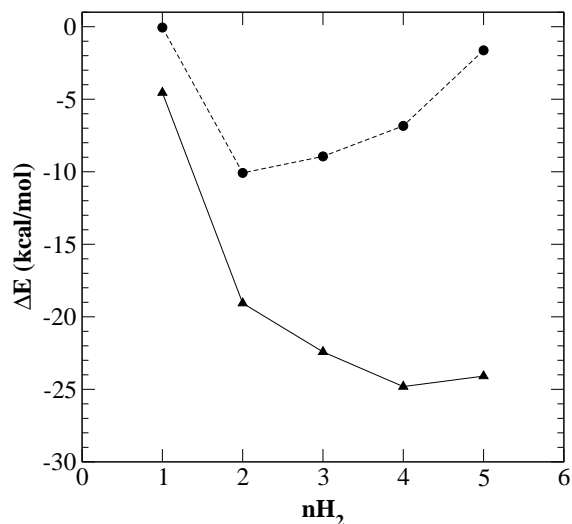
Figure 4.3. Reaction energies (ΔE) as a function of guest H_2 occupancy in the large cage at 1 atm (dotted line) and at 2000 bar (solid line). All calculations are performed with MP2/6−311+G* level of theory.

the cage, and the remaining space is considered free. The occupancy is then determined by placing dumbbell-type H_2 molecules with radii 1.0 Å into the available volume. It was possible to fit three hydrogen molecules into the small cavity while five would fill the larger cavity. If free volume were the limiting factor, the filling capacity of the clathrate cages would be significantly higher. Therefore, repulsive forces between the guest hydrogen molecules and between the guest hydrogen and water molecules of the cage must play a significant role in the occupancy of these clusters.

4.4   Conclusions

Alavi and coworkers[9] reported that classical molecular dynamics simulations obtained a single H_2 occupancy in the small cage, whereas earlier quantum chemical studies obtained two presumably because the classical model allowed for flexibility of the cage and included cooperative effects from the neighboring cages.[9] This work demonstrates that quantum chemical calculations also predict single occupancy of the small cage, even without these considerations in the model if a large basis set is employed. More importantly, this work unifies the results of quantum calculations and molecular dynamics simulations, making both methods valid for determination of hydrogen occupancy of the clathrate cages.

Acknowledgment

References

[1] E. D. Sloan. *Clathrate Hydrates of Natural Gases*. Marcel Dekker Inc., New York, 2nd edition, 1998.

[2] Y. A. Dyadin, E. D. Larinov, A. Y. Manakov, F. V. Zhurko, E. Y. Aladko, T. V. Mikina, and V. Y. Komarov. *Mendeleev Commun.*, 5:209, 1999.

[3] W. L. Mao, H.-K. Mao, A. F. Goncharov, V. V. Struzhkin, Q. Guo, J. Hu, J. Shu, R. J. Hemley, M. Somayazulu, and Y. Zhao. *Science*, 297:2247, 2002.

[4] W. L. Mao and H.-K. Mao. *Proc. Natl. Acad. Sci. U.S.A.*, 101:708, 2004.

[5] S. Patchkovskii and J. S. Tse. *Proc. Natl. Acad. Sci. U.S.A.*, 100:14645, 2003.

[6] B. C. Chakoumakos, C. J. Rawn, A. J. Rondinone, L. A. Stern, S. Circone, S. H. Kirby, Y. Ishii, C. Y. Jones, and B. H. Toby. *Can. J. Phys.*, 81:183, 2003.

[7] M. H. F. Sluiter, H. Adachi, R. V. Belosludov, V. R. Belosludov, and Y. Kawazoe. *Mater. Trans.*, 45:1452, 2004.

[8] K. A. Lokshin, Y. Zhao, D. He, W. L. Mao, H.-K. Mao, R. J. Hemley, M. V. Lobanov, and M. Greenblatt. *Phys. Rev. Lett.*, 93:125503, 2004.

[9] S. Alavi, J. A. Ripmeester, and D. D. Klug. *J. Chem. Phys.*, 123:024507, 2005.

[10] E. A. Smelik and H. E. King. *Z. Kristallogr.*, 211:84, 1996.

[11] R. T. Cygan, S. Guggenheim, and A. F. K. van Groos. *J. Phys. Chem. B*, 108:15141, 2004.

[12] G. Kresse and J. Hafner. *Phys. Rev. B*, 47:RC558, 1993.

[13] G. Kresse and J. Furthmüller. *Phys. Rev. B*, 54:11169, 1996.

[14] K. Burke, J. P. Perdew, and Y. Wang. In J. F. Dobson, G. Vignale, and M. P. Das, editors, *Electronic density functional theory: Recent progress and new directions*. Plenum Press, New York, 1998.

[15] J. P. Perdew. In P. Ziesche and H. Eschrig, editors, *Electronic structure of solids '91*. Akademie Verlag, Berlin, 1991.

[16] J. P. Perdew, K. Burke, and Y. Wang. *Phys. Rev. B*, 54:16533, 1996.

[17] J. P. Perdew, J. A. Chevary, S. H. Vosko, K. A. Jackson, M. R. Pederson, D. J. Singh, and C. Fiolhais. *Phys. Rev. B*, 46:6671, 1992.

[18] J. P. Perdew, J. A. Chevary, S. H. Vosko, K. A. Jackson, M. R. Pederson, D. J. Singh, and C. Fiolhais. *Phys. Rev. B*, 48:4978, 1993.

[19] M. J. Frisch, et al. Gaussian 98, 1998. revision A.2; Gaussian, Inc., Pittsburgh, PA.

[20] A. D. Becke. *J. Chem. Phys.*, 98:5648, 1993.

[21] C. Lee, W. Yang, and R. G. Parr. *Phys. Rev. B*, 37:785, 1988.

[22] R. Krishnan, J. S. Binkley, and J. A. Pople. *J. Chem. Phys.*, 72:650, 1980.

[23] A. D. McLean and G. S. Chandler. *J. Chem. Phys.*, 72:5639, 1980.

[24] C. Möller and M. S. Plesset. *Phys. Rev.*, 46:618, 1934.

[25] K. D. Dobbs and W. J. Hehre. *J. Comput. Chem.*, 7:359, 1986.

[26] K. D. Dobbs and W. J. Hehre. *J. Comput. Chem.*, 8:861, 1987.

[27] K. D. Dobbs and W. J. Hehre. *J. Comput. Chem.*, 8:880, 1987.

[28] J. S. Binkley, J. A. Pople, and W. J. Hehre. *J. Am. Chem. Soc.*, 102:939, 1980.

[29] M. S. Gordon, J. S. Binkley, J. A. Pople, W. J. Pietro, and W. J. Hehre. *J. Am. Chem. Soc.*, 104:2797, 1982.

[30] W. J. Pietro, M. M. Francl, W. J. Hehre, J. A. Pople, and J. S. Binkley. *J. Am. Chem. Soc.*, 104:5039, 1982.

[31] R. Voorintholt, M. T. Kosters, G. Vegter, G. Vriend, and W. G. J. Hol. *J. Molec. Graphics*, 7:243, 1989.

[32] E. V. Stefanovic and T. N. Truong. *Chem. Phys. Lett.*, 244:65, 1995.

[33] P. J. Feibelman. *Science*, 295:99, 2002.

DISTRIBUTION:

1 MS 0734
Chris Cornelius, 6338

1 MS 0734
Mike Hickner, 6338

1 MS 0734
Ellen Stechel, 6338

1 MS 0735
John Merson, 6300

1 MS 0754
Patrick Brady, 6316

1 MS 0754
Louise Criscenti, 6316

1 MS 0754
Randall Cygan, 6316

1 MS 0754
Jeff Greathouse, 6316

2 MS 0886
Todd Alam, 1816

1 MS 0888
Cy Fujimoto, 6338

1 MS 0895
Marcus Martin, 8333

3 MS 0895
Susan Rempe, 8333

1 MS 1110
Jeff Nelson, 6337

1 MS 1303
Gary Grest, 1133

1 MS 1316
Danny Rintoul, 1412

1 MS 1322
John Aidun, 1435

1 MS 1349
John Shelnutt, 1112

1 MS 1411
Bruce Bunker, 1816

1 MS 1411
Eliot Fang, 1814

1 MS 1413
Kathe Andrews, 8333

1 MS 1413
Grant Heffelfinger, 8330

1 MS 1413
Dubravko Sabo, 8333

1 MS 1413
Sameer Varma, 8333

1 MS 1415
Kevin Leung, 1133

1 MS 1415
Tina Nenoff, 1133

1 MS 9052
Jay Keller, 8367

1 MS 9054
Don Hardesty, 8360

1 MS 9054
Terry Michalske, 8300

1 MS 9161
Sarah Allendorf, 8756

1 MS 9161
Roland Stumpf, 8756

1   MS 9292   Blake Simmons, 8755

2   MS 9018   Central Technical Files, 8944

2   MS 0899   Technical Library, 4536

1   MS 0123   D. Chavez, LDRD Office, 1011